"Characterizing the Crystallization of the D1D2 Heterodimer using Microfluidic Devices"

Bachelorarbeit

vorgelegt von

Markus Ludwig

an der

Universität Konstanz

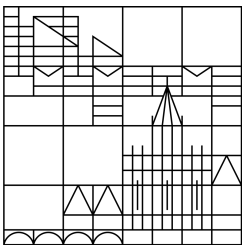

Fachbereich Physik

angefertigt an der *Brandeis University* in Waltham, Massachusetts, USA

1. Gutachter: Prof. Dr. Georg Maret
2. Gutachter: Prof. Dr. Seth Fraden

Bearbeitungszeitraum: 15. Mai 2012 - 15. Oktober 2012

Konstanz, im Oktober 2012

Erklärung

Ich versichere hiermit, dass ich diese Arbeit selbstständig verfasst und keine anderen Hilfsmittel als die angegebenen benutzt habe. Die Stellen, die anderen Werken dem Wortlaut oder dem Sinne nach entnommen sind, habe ich in jedem einzelnen Falle durch Angaben der Quelle, auch der benutzten Sekundärliteratur, als Entlehnung kenntlich gemacht. Als Urheber dieser Arbeit stimme ich der Übergabe an die Universitätsbibliothek vorbehaltlich des abgeschlossenen Patentverfahrens nicht zu.

Konstanz, den 5. Oktober 2012

1 Zusammenfassung

Die Struktur von Proteinmolekülen hat sich als hilfreiches Werkzeug in der Entwicklung neuer Medikamente und zum Verständnis von biologischen Prozessen erwiesen. Sie kann mithilfe von Röntgenbeugung an einem Kristall des entsprechenden Proteins bestimmt werden. Die Herstellung der Proteinkristalle stellt einen Engpass dar, denn Proteine sind oftmals nur in sehr begrenzten Mengen verfügbar und lassen sich nicht nach einem einheitlichen Rezept kristallisieren. Es müssen aufwändige Verfahren zur Bestimmung der optimalen Bedingungen bemüht werden. Der Weg von einer Proteinlösung zum Proteinkristall besteht aus zwei Schritten: Bei der Nukleation bildet sich ein Keim, der in der folgenden Wachstumsphase zum Kristall heranwächst. Der wichtigste Parameter ist hierbei die Übersättigung, mit welcher sich der gesamte Prozess steuern lässt. Die Nukleation erfordert eine vergleichsweise hohe Übersättigung, während eine vergleichsweise niedrige Übersättigung für ein defektvermindertes Kristallwachstum nötig ist. Keine der bisher bekannten und angewandten Kristallisationsmethoden ermöglicht eine Entkopplung von Nukleation und Wachstum. Lediglich beim sogenannten seeding werden Keime aus einer stark übersättigten Lösung in eine leicht übersättigte Lösung transferiert. Diese Methode ist jedoch in ihrer Anwendung sehr aufwändig.

Die in dieser Arbeit behandelte Methode des mikrofluidischen Phasenchips ermöglicht es, die Übersättigung im Kristallisationsexperiment kontinuierlich zu steuern. Der Phasenchip besteht aus 288 in einer Matrix angeordneten Kammern von ca. 20 nL, die jeweils mit der Proteinlösung befüllt werden. Diese Probentröpfchen interagieren osmotisch mit einem Reservoir durch eine Membran. Da sich die chemischen Potentiale der Tröpfchen jeweils lokal dem des Reservoirs anpassen, können deren chemische Potentiale durch eine Manipulation des Reservoirs gezielt verändert werden, um die Übersättigung der Proteinlösung zu beeinflussen. Ferner ermöglicht der Einsatz eines sogenannten graduierten Reservoirs das Anlegen einer Verteilung verschiedener chemischer Potentiale über die Spalten der Probenmatrix. Durch die optionale Verwendung eines Temperaturgradienten über die Zeilen der Matrix können so Phasendiagramme bis in zwei Dimensionen bestimmt werden.

Diese Arbeit beschäftigt sich mit der Charakterisierung eines neuen Entwurfs des Phasenchips, welcher eine Dialysemembran einsetzt. Im Vergleich zu der bereits veröffentlichen Version ermöglicht die Dialysemembran neben dem Austausch von Wasser auch den Austausch von Ionen, pH Puffern oder sogar Polymeren. Es kann damit nicht nur der Wasserhaushalt, sondern auch die Zusammensetzung der Proteinlösungen gesteuert werden.

Um die Anwendung dieses neuen Phasenchips zu ermöglichen, war ein Ziel dieser Arbeit die Entwicklung von Anwendungspraktiken. Es wurden Transportflüsse von Wasser durch die Membran in Abhängigkeit hydrostatischer und osmotischer Drücke untersucht, die ein gezieltes Anschwellen oder Schrumpfen der Probentröpfchen ermöglichen. Ein elektrisches Widerstandsnetzwerk hat sich als gutes Modell für die experimentellen Beobachtungen erwiesen. Bedingungen zur optimalen Funktion des graduierten Reservoirs

wurden ermittelt. Sein hydrodynamischer Widerstand wurde gemessen, um für dessen korrekte Funktion maximal erlaubte Flussraten in Abhängigkeit der Diffusionskonstanten der verwendeten Lösungen abzuschätzen. Um die Tauglichkeit des neuen Phasenchips zur Kristallisation von Proteinen zu verifizieren, wurden Glucose Isomerase Kristalle gezüchtet und deren Qualität in einem Syncrotron untersucht. Die neuen Erkenntnisse wurden im Versuch angewandt, ein eindimensionales Phasendiagramm des D1D2 Heterodimers in Abhängigkeit des pH-Wertes zu erstellen.

Contents

2 Abstract

To crystallize proteins is the bottleneck in determining their molecular structure by x-ray diffraction. In protein crystallization, vapor diffusion or batch methods are employed most commonly, though both these techniques cannot decouple crystal nucleation from growth. In this thesis, a microfluidic phase chip method is explored in which the kinetic path of the crystallization process can be controlled reversibly by manipulating protein supersaturation over time. The chip has hundreds of 20 nanoliter-sized sample wells arranged in a two dimensional matrix. In this thesis, the phase chip method was extended to allow the incorporation of a dialysis membrane to exchange water, ions and even polymer between the reservoir solution and the protein samples under investigation. This approach allows to selectively quench composition and thus supersaturation levels and to apply spatial gradients across an array of hundreds of samples using osmosis and reverse osmosis. The chip can be used to map phase diagrams of a protein, to optimize the crystallization kinetics and to systematically grow crystals using optimized receipes. To establish standard operating procedures for the new device, transport fluxes of water between the sample and the reservoir were characterized as a function of hydrostatic and osmotic pressures. A model was derived to predict fluxes depending on the hydrostatic pressures applied. The proper functioning of the reservoir was tested and its hydrodynamic resistance was determined to allow the estimation of maximal flow-rates, based on diffusion constants of reservoir solutions. Glucose isomerase crystals grown in the chip were harvested and their quality was analyzed by x-ray diffraction. It was attempted to map a 1-dimensional phase diagram of varying pH of the D1D2 heterodimer.

3 Theory

3.1 The Importance of Protein Crystallization

Solving the structure of a protein brings huge benefits in understanding its function, which for example is required to rationally design dedicated pharmaceuticals. To determine the structure of proteins, it is necessary to collect x-ray diffraction patterns from its crystals. From the diffraction data, the electron distribution of the molecule can be reconstructed. It is wishful to have crystals of ideally best quality with no defects to obtain the highest resolution possible. [Leu01]

3.2 Classical Nucleation Theory

Protein molecules in a solution act as the building blocks for a crystal. They diffuse in the solvent, collide with each other. This results in protein density fluctuations over time and space. By chance, a small cluster - a nucleus - may form.

The excess free energy ΔG of such a nucleus can be expressed as:

$$\Delta G = \Delta G_{surface} - \Delta G_{volume} \quad (1)$$
$$= A\epsilon - n(\mu_{solution} - \mu_{liquid}). \quad (2)$$

$\Delta G_{surface}$ is the product of the specific energy ϵ and the surface A of the nucleus. ΔG_{volume} accounts for the difference in chemical potential that arises when n molecules are moved from the liquid to the solid crystal phase.

The chemical potentials can be written as

$$\mu_{solution} = kT\ln(c_{liquid}), \quad (3)$$

and

$$\mu_{solid} = kT\ln(c_{solid}), \quad (4)$$

where c are the respective concentrations of protein molecules in solution or in the solid phase. Supersaturation S can be defined as the ratio of these concentrations:

$$S = \frac{\mu_{liquid}}{\mu_{solid}}. \quad (5)$$

With the help of Equation 5 and 4, this can be brought to

$$\mu_{solution} - \mu_{solid} = kTln(S) \quad (6)$$

Substitution into Equation 1 yields the expression:

$$\Delta G = -n\,(kTln(S)) + A\epsilon \quad (7)$$

For a spherical nucleus at a radius r and the definition of v for the volume of one protein molecule, we obtain:

$$\Delta G = \frac{4\pi r^3}{3v}kTln(S) + 4\pi r^2\epsilon. \quad (8)$$

ϵ has to be expressed in the form $\sum A_i\epsilon_i$, since different faces of the crystal might have different surface energies.

Forming the derivative of ΔG shows that there is one maximum at

$$r_{crit} = \frac{2v\epsilon}{kTln(S)} \quad (9)$$

This is the so-called critical radius. A specific energy corresponding to this critical radius has to be overcome to grow a crystal from a nucleus:

$$\Delta G_{crit} = \frac{16\pi v^2\epsilon^3}{3(kT\ln(S)^2)} \quad (10)$$

Energy is consumed to form and grow a nucleus until its size surpasses the critical radius. After this, energy is gained from

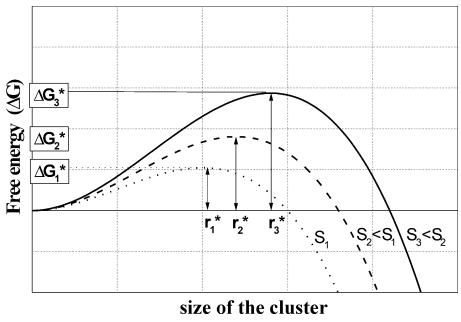

Figure 3.1: *Critical radius and nucleation barrier for different supersaturations S: Lower supersaturation increases the nucleation barrier and critical radius. (Image from [GR03])*

further growing the nucleus. Increased supersaturation lowers this energy barrier (nucleation barrier) and also r_{crit}, as indicated in Figure 3.1.

According to Boltzmann's distribution law, there is a relationship between the ratio of the number of particles in two different energy states and the energy difference between these two states. In this case, the energy difference is ΔG and the number of particles in the liquid and the solid phase are N_0 and N_1:

$$\ln\left(\frac{N_1}{N_0}\right) = \frac{-\Delta G}{kT} \tag{11}$$

[phy]. Based on this equation, a relationship for the nucleation rate J can be formed

$$J = C \cdot \exp\left(\frac{-\Delta G}{kT}\right), \tag{12}$$

where C is a parameter that describes the kinetics of free molecules joining the nucleus. The nucleation rate describes the frequency of nucleation to happen. Substitution of Equation 10 gives

$$J = A \exp\left(\frac{-16\pi v^2 \epsilon^3}{3(kT^3) ln(S)^2}\right) \tag{13}$$

A supersaturation of $S = 1$ (saturation) results in a nucleation rate of $J = 0$. Slightly increasing supersaturation does not significantly increase the nucleation rate. This is often referred to as the "metastable zone". This term can be confusing, since nucleation is a stochastic process and thus, any supersaturation $S > 0$ results in a nucleation rate $J > 0$, which even though might be very small. The width of the metastable zone that is indicated in Figure 3.2 is thus in the eye of the experimentator. Above a certain critical supersaturation S^*, the nucleation rate increases rapidly, since thermal fluctuations in this zone are in the order of magnitude of the nucleation barrier. This is referred to as the "labile zone". [GR03]

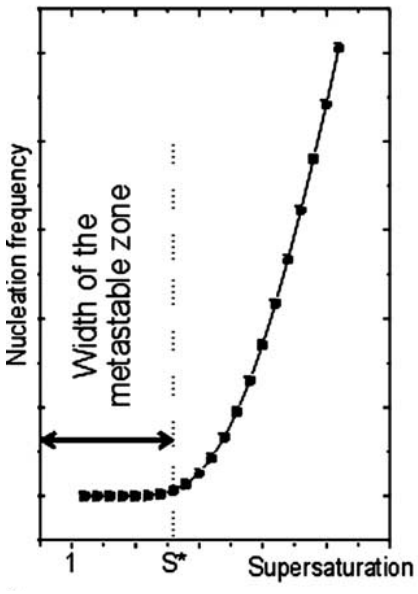

Figure 3.2: *Nucleation frequency versus supersaturation: Above a critical supersaturation S^*, the nucleation frequency increases rapidly. The width of this "metastable zone" is in the eye of the experimentator since any supersaturation $S > 0$ results in a nucleation rate $J > 0$. (Image from [GR03])*

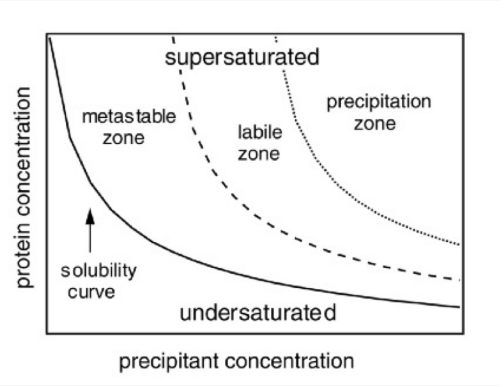

Figure 3.3: *Depending on the protein- and precipitant concentrations, different zones of supersaturation can be defined. The border between the labile zone and the metastable zone is in the eye of the experimentator. The solubility curve and the precipitation zone are defined physically. (Image from [Ash04])*

3.3 Enhancing Crystal Quality by Decoupling Nucleation and Growth

While high supersaturation favors nucleation, a low supersaturation is favorable for growing crystals and to inhibit secondary nucleation events. High supersaturation also translates into fast crystal growth, where defects are more likely to occur [Sel10]. Nucleation and growth have to be decoupled in order to obtain crystals of best quality. One approach to solve this problem is transferring nuclei of a proper size from a solution of high supersaturation into a solution of low supersaturation, referred to as "seeding" [Ber03]. Another approach is the microfluidic phase chip method investigated in this thesis, which allows to control and adjust supersaturation throughout the experiment [SJF09].

3.4 Parameters that Influence Protein Crystallization

Supersaturation profoundly affects crystal nucleation and growth. It is influenced by various parameters:

Protein Concentration: Increasing the protein concentration directly increases supersaturation, as this changes the ratio in Equation 5.

Temperature: Solubility of the protein usually increases with rising temperature, or lowers with decreasing temperature. A change of the solubility also affects supersaturation directly. However, cases for retrograde solubility are known, too [RHSN93].

Salts: From low to medium concentration, salt ions elevate the dielectric constant of the solvent and increase solubility of the protein or lower its supersaturation (referred to as "salting in"). From medium to high ionic strength, solubility decreases, since the charges compete with the protein for solvent molecules, which is equal to increasing the concentration of protein or increasing supersaturation ("salting out"). [mit]

pH: The solubility of a protein is lowest at the so-called isoelectric point: At a specific pH level, the protein does not carry any net charge and the attractive forces between the protein and polar water molecules are at a minimum, resulting in low solubility. Lowering or increasing the pH level from the isoelectric point increases the net charge and thus the solubility and lowers supersaturation of the protein. [MHA00]

Polymers: Polymers act as a crowding agent, utilizing the depletion mechanism described in [AO54]. Increasing polymer concentration increases attractive forces between the protein molecules and therefore

increases the supersaturation. Especially polyethyleneglycol (PEG) is a very common precipitant for proteins. The radius of gyration of the polymer molecule, that is related to its molecular weight, sets the range of the attractive potential [VBTB02]. Usually PEG of a molecular weight between 1000 and 10000 kDa is used for protein crystallization [KZ01].

3.5 Quality-Parameters for a Crystal

When crystals are analyzed in x-ray diffraction, there are two major parameters that indicate the quality of a crystal:

3.5.1 Mosaicity

Protein crystals can have various imperfections. A crystal could be considered as an accumulation of a huge number of small and perfect crystals, that can have a slight translational and rotational variation in their position relative to the perfect crystal lattice. Mosaicity indicates the average angle of misorientation of these small crystals. High mosaicity therefore broadens or smears the diffraction spots, causing spot overlap and a reduced diffraction [elv]. Crystals with low mosaicity are therefore preferred for structure determination.

3.5.2 Resolution Obtained from a Crystal

When a map of a protein is constructed from diffraction data, this map represents the electron density within the protein molecule. The resolution of a crystal describes the shortest distance in reciprocal space, that can be obtained in the diffraction experiment [elv]. The goal is to grow crystals with lowest defects that diffract to the highest possible resolution.

3.6 Conventional Methods for Protein Crystallization

The two most common protein crystallization methods are batch crystallization and vapor diffusion [Leu01]:

3.6.1 Microbatch Crystallization

In microbatch crystallization, the protein solution is mixed with mother liquor (buffer and precipitant), placed in a small well and surrounded with paraffin oil, preventing evaporation. The initial formulation needs to be located in the labile zone in order to achieve crystallization (Figure 3.5) [Leu01]. Nucleation and growth require contrary supersaturation conditions, which is not taken into account in this method.

3.6.2 Vapor Diffusion

There are several variations of vapor diffusion methods, that are based on the same principle: A droplet of an undersaturared protein solution can exchange water vapor with a reservoir solution through air (Figure 3.5). Vapor equilibration will then slowly reach supersaturation within the droplet, that allows nucleation and growth. The advantage towards the batch method is that in vapor diffusion, the protein slowly reaches supersaturation which helps to avoid shock nucleation that produces showers of crystals or even precipitation [Leu01]. This method also does not respect different requirements for nucleation and growth.

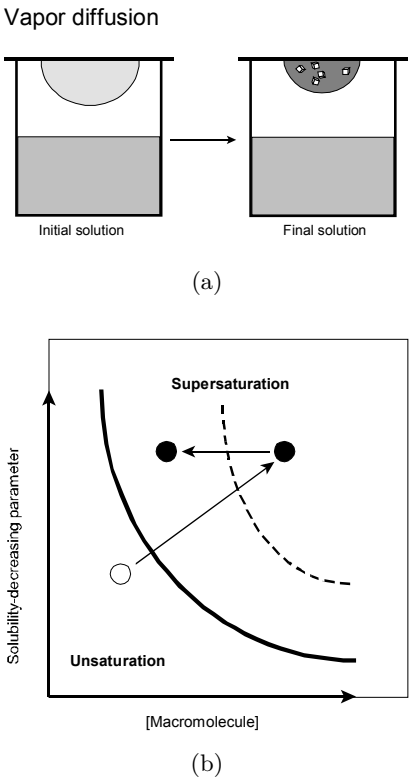

Figure 3.4: *Sketch of vapor diffusion method: (a) Water vapor can exchange between a reservoir solution and the droplet of a protein solution. Thus, supersaturation increases slowly until nuclei are formed. (b) Kinetic path of vapor diffusion method: Initial supersaturation decreases from the labile zone to the metastable zone due to the formation of crystals. (Images from [Leu01])*

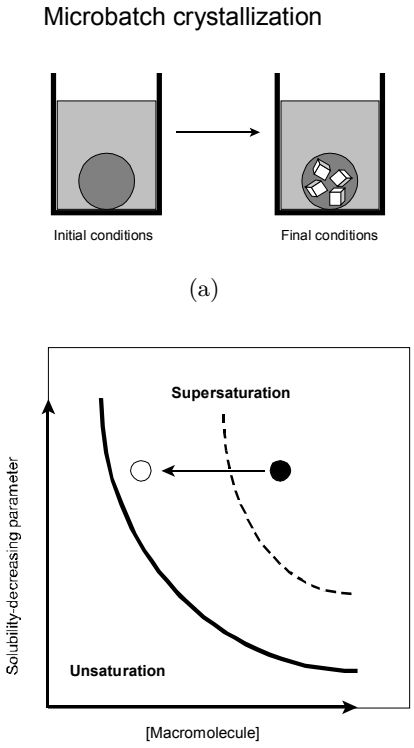

Figure 3.5: *Sketch of microbatch method: (a) The supersaturated protein solution is surrounded with paraffin oil. (b) Kinetic path of batch method: Initial supersaturation decreases from the labile zone to the metastable zone due to the formation of crystals. (Images from [Leu01])*

3.7 Characteristics of Microfluidics

Microfluidics promises to revolutionize biotechnology, medical engineering and process technology similar to how miniaturization of integrated circuits revolutionized computation [TMS05]. It deals with the bahaviour of small volumes of liquids constrained to small geometries. Technologies have been and are being developed to control, manipulate and store small amounts of liquids. Typical sizes in microfluidics are micrometers and typical volumes are nanoliters. One application are lab-on-a-chip devices that incorporate functions of a laboratory into a device in the size of square centimeters (Figure 3.6) [loa].

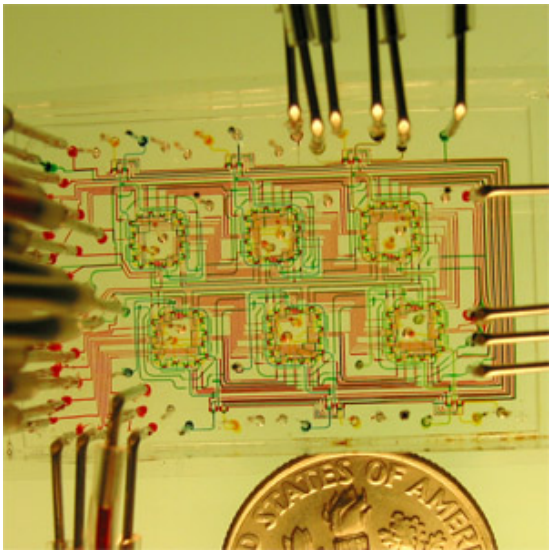

Figure 3.6: *Lab on a chip devices incorporate the functionality of a laboratory into the size of square centimeters. (Image from [nan])*

Low Reynolds Number: Laminar Flow The Reynolds Number describes the relationship between inertial forces f_i and viscous forces f_v in a fluid:

$$\frac{f_i}{f_v} \propto \frac{\frac{\rho U^2}{L^2}}{\frac{\eta U}{L^2}} = \tag{14}$$

$$= \frac{\rho \cdot U \cdot L}{\eta} = Re, \tag{15}$$

where U is the mean velocity of the fluid relative to the object, L the length that the fluid travelled, ρ its density and η the dynamic viscosity. It was observed experimentally that $Re < 2200$ results in laminar flow and $Re > 2200$ yields turbulent flow [Dem05]. In microfluidics, typical Reynolds numbers are in the order of 10^{-6} to 10. Hence, flow in microfluidic devices is laminar. [TMS05]

Poiseuille Flow: In laminar flow, Hagen Poiseuille's Law can be applied to estimate flow-rates in a channel as a function of viscosity η and the pressure difference Δp between its ends. In a channel with a circular cross-section of the radius R and the length L, the flow-rate is

$$I = \frac{\pi R^4 \Delta p}{8 \eta L} \tag{16}$$

[Dem05]. From this equation, a specific flow resistance C can be defined:

$$I = C \cdot \frac{\Delta p}{\eta}. \tag{17}$$

Once the flow resistance of a specific channel was determined experimentally, the flow can be calculated depending on Δp and η.

3.8 Osmosis and Reverse Osmosis

Osmosis is a thermodynamic process in which two solutions of different chemical potentials are seperated by a membrane, that is

only permeable to the solvent. Osmosis will exchange the solvent between the two solutions to equilibriate their concentrations or their chemical potentials. When a reservoir of a solution of a molar concentration c is connected to a reservoir containing the pure solvent, a pressure will build up in the solution that tries to equilibriate concentrations. This so-called osmotic pressure can be calculated by Van't Hoff's formula:

$$p = c \cdot R \cdot T \tag{18}$$

[Mes06], where n is the number of molecules, V the Volume, $R = 8.3144621 \frac{J}{molK}$ the universal gas constant and T the temperature. The osmotic pressure depends only on the osmolarity $c = \frac{n}{V}$, but not on the nature of the molecules.

When the pressure inside the solvent is increased by external influences, it is possible to force the solvent through the membrane, overmatching the osmotic pressure of the solution in the other reservoir. This process is called reverse osmosis. Osmosis and reverse osmosis are both utilized in the phase chip method.

4 The Phase Chip

The phase chip method can modulate protein supersaturation reversibly, by "surfing" the phase diagram. Any desired kinetic path can be applied to a sample. In this section, the concept of a novel dialysis phase chip method is introduced. Compared to the previous permeation-based decvice [SGF12], the new device is modular, reusable and employs a dialysis membrane instead of a PDMS membrane, which offers multiple advantages.

The phase chip consists of two microfluidic layers that are separated by a semipermeable membrane and a perforated Teflon foil. The storage layer on the very top is a matrix of 288 storage wells that each can hold an isolated protein solution sample (Figure 4.1 (a)). These sample droplets can interact osmotically through a dialysis membrane with a reservoir solution perfused in the reservoir layer that is located at the bottom of the chip: Water and solutes can diffuse through the membrane between sample droplet and reservoir (Figure 4.1 (c)). Depending on the molecular weight cut-off of the membrane, ions, acids, bases or bigger molecules such as pH-buffers or even polymers can diffuse across the membrane. The sample droplets always react in a way that thermodynamic equilibrium towards the reservoir solution underneath is reached. The reservoir solution is being refreshed constantly, causing the droplets to adopt the osmotic pressure of the reservoir solution by the exchange of water and other molecules, but not protein molecules. This allows to reversibly vary the formulation of the protein samples: If for example the ionic strength in the droplets should be first increased and then later lowered again, this can be achieved by first flushing a solution of the desired high ionic strength and then later followed by one of lower ionic strength through the reservoir layer. The sample droplets will converge towards the currently applied ionic strength of the reservoir solution and thus follow the temporal trajectory. In the previous version of the phase chip, a PDMS membrane was used that was only permeable to water.

The chip is a clamped assembly, where the storage layer is made from polyurethane and the reservoir from PDMS. The flexible PDMS reservoir is mechanically supported by a plexiglass bottom piece to provide a

good seal.

In this modular design, different types of reservoir designs can be used. The simplest reservoir is a *constant reservoir*, that provides the same reservoir solution to every sample droplet in the matrix. When mapping phase diagrams, it is necessary to use a *gradient reservoir*, which can provide a defined range of conditions across the storage layer. If for example the pH on a crystallization trial should be examined, a gradient reservoir can deliver a distribution of pH values across the columns of droplets in the sample matrix. It is also possible to apply a temperature gradient across the rows of the matrix (Figure 4.1 (b)).

The images in Figure 4.2 show the components of the new phase chip. Instructions on how to manufacture, set up and load the phase chip can be found in Section 10.

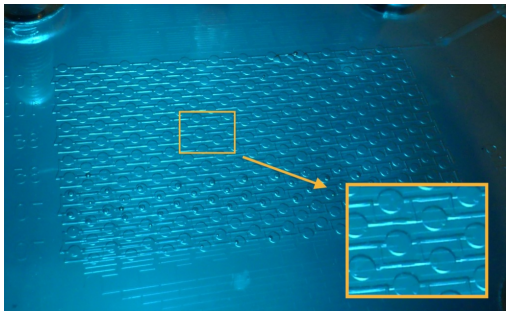

(a)

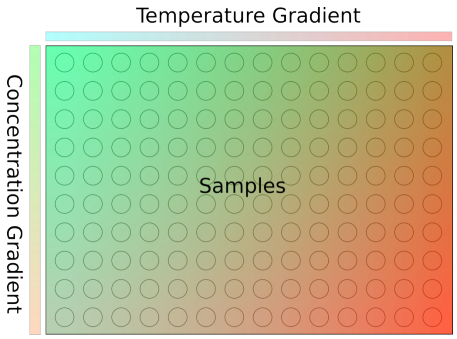

(b)

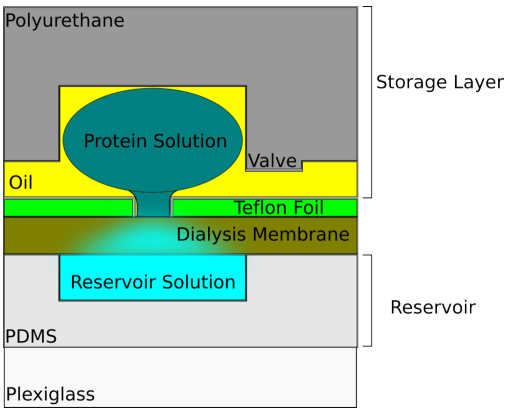

(c)

Figure 4.1: *The phase chip method: Protein solution is loaded into a matrix of 288 storage wells (a). Each storage well is 600μm in diameter and can hold about 20nl. A combination of a concentration and a temperature gradient can be applied to the samples in a single operation to map 2-dimensional phase diagrams quickly (b). Storage layer and reservoir layer can communicate across a dialysis membrane. Cross-section of the phase chip (a), not true to scale.*

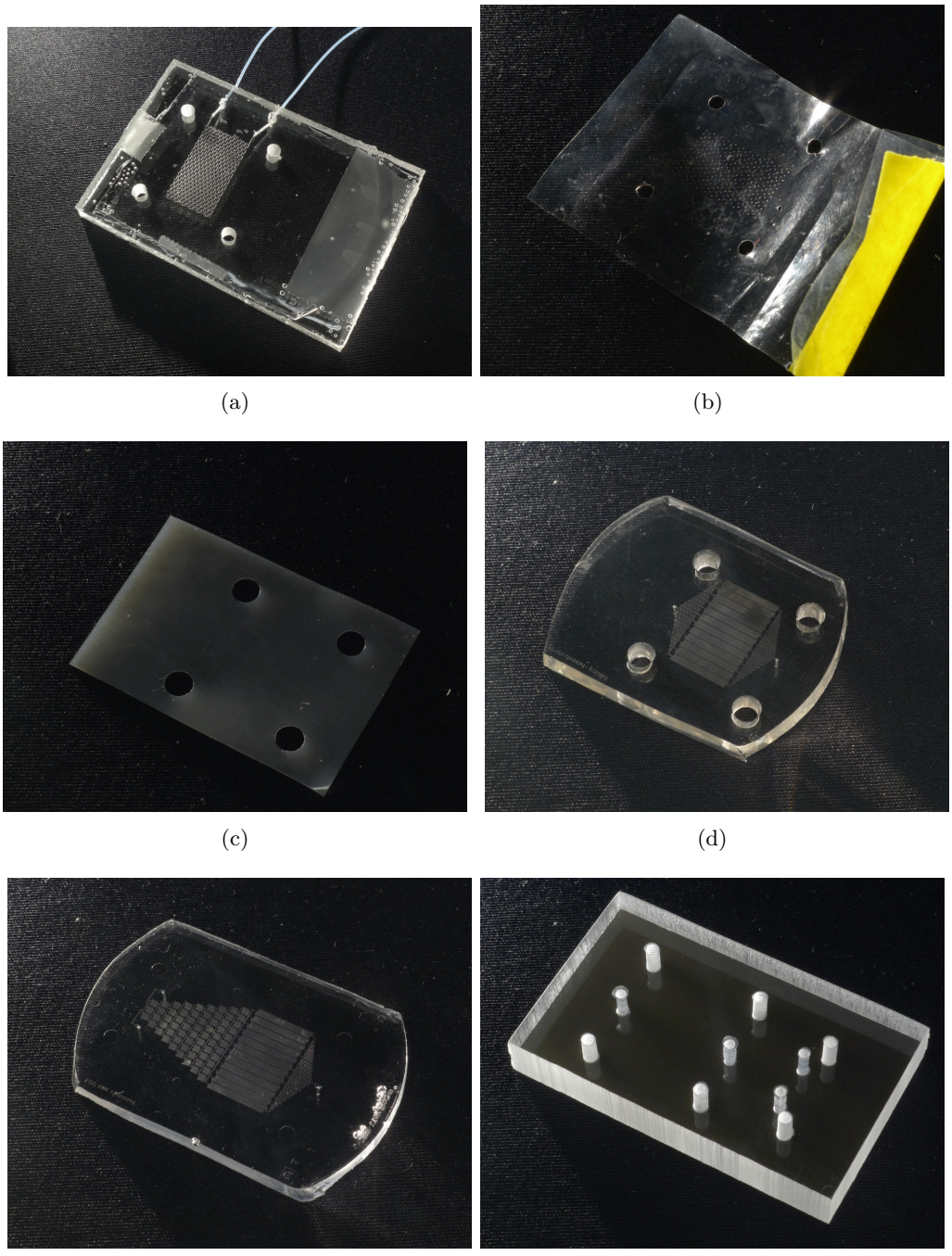

(a) (b)

(c) (d)

(e) (f)

Figure 4.2: *Components of the phase chip: (a) storage layer, (b) microperforated Teflon foil, (c) membrane, (d) constant reservoir, (e) gradient reservoir, (f) plexiglass bottom piece. The side length of the four circles arranged in a square is 26 mm.*

4.1 Loss-Free Sample Loading Using Capillary Valving

The loading process is a loss-free process, which means that no waste is being produced from the precious sample solution. After the loading, there are 288 independent samples droplets stored in the storage layer matrix. To load all 288 storage wells, a total volume of less than $6\mu l$ of a sample is required. These two properties are ideal for protein crystallization, where the amount of available protein is often limited. The process utilizes the principle of capillary valving, that was first published in [BSJ+09]. This section explains the loading mechanism.

Inside the drop of a liquid, a pressure will build up caused by the surface tension of the liquid. The smaller the drop, the bigger this so-called Laplace pressure, that can be calculated by the Young Laplace equation given by

$$\Delta p = \epsilon \left(\frac{1}{R_x} + \frac{1}{R_y} \right), \qquad (19)$$

where R_1 and R_2 are the main radii of curvature of the droplet surface and ϵ the surface tension of the liquid in the medium. [Skj06] In order to minimize its surface energy, the droplet tries to minimize its surface which is equivalent to maximizing its main radii of curvature at a constant volume.

The storage wells are designed as cylindrical cavities and connected in series by a long serpentine channel. The design is shown in Figure 4.3. Prior to the loading procedure, the whole storage layer is primed with oil. Then, the sample slowly gets flushed through the channel. The subtle idea behind the loading procedure is that there are three different cross-sectional areas a, b and c involved in the microfluidic design as indicated in Figure 4.3. The dimensions of the respective crossectional areas are $a = 70\mu m \cdot 100\mu m$, $b = 70\mu m \cdot 75\mu m$ and $c = 25\mu m \cdot 100\mu m$. In order to pass through these sections, the biggest curvature or lowest pressure for a liquid is needed when passing through section a, followed by b and finally c. When driven by constant flux, the aqueous solution will therefore fill the storage well first while displacing the oil from it and then pass around the storage well towards the following storage wells. The solution will never enter section c.

If we assume we want to load the chip at constant pressure and set the pressure to a value that just allows the solution to enter section a, the storage well would be filled with the solution, while displacing the oil through section c. After filling the well completely, the flow would stop because a higher pressure is needed to force the aqueous solution through section b and especially c. Increasing the pressure such that the solution can also pass section b allows the solution to pass through section a and b at the same time, causing several storage wells to be loaded at the same time. This would make the loading process unpredictable and the amount of solution deposited in the wells would vary a lot. The loading at constant pressure thus does not work properly. It is important to use constant flux for loading the chip because this ensures that only one storage well is filled at a time.

When the incoming aqueous phase ends, oil enters the chip. It fills the channels between the storage wells, leaving the aqueous solution inside them. Once all channels are filled with oil, it blocks the “cross-talk” between the sample droplets in the storage matrix.

Hence, 288 individual sample droplets were produced that have almost the exact same volumes. Images of loading the phase chip can be found in Figure 4.4.

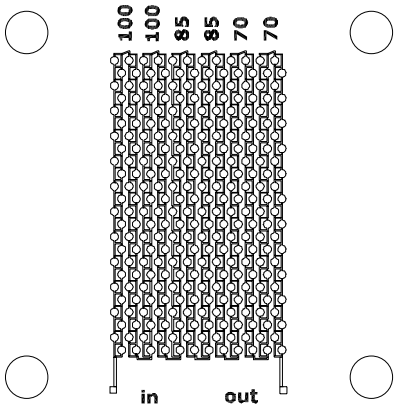

(a)

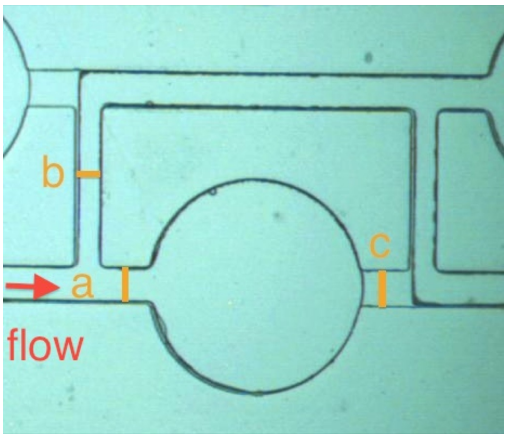

(b)

Figure 4.3: *Design of the reservoir layer: (a) 288 wells are connected in series. The side length of the four circles arranged in a square is 26 mm. (b) Three different crossectional areas were established in the design for capillary valving:* $a = 70\mu m \cdot 100\mu m$, $b = 70\mu m \cdot 75\mu m$ *and* $c = 25\mu m \cdot 100\mu m$

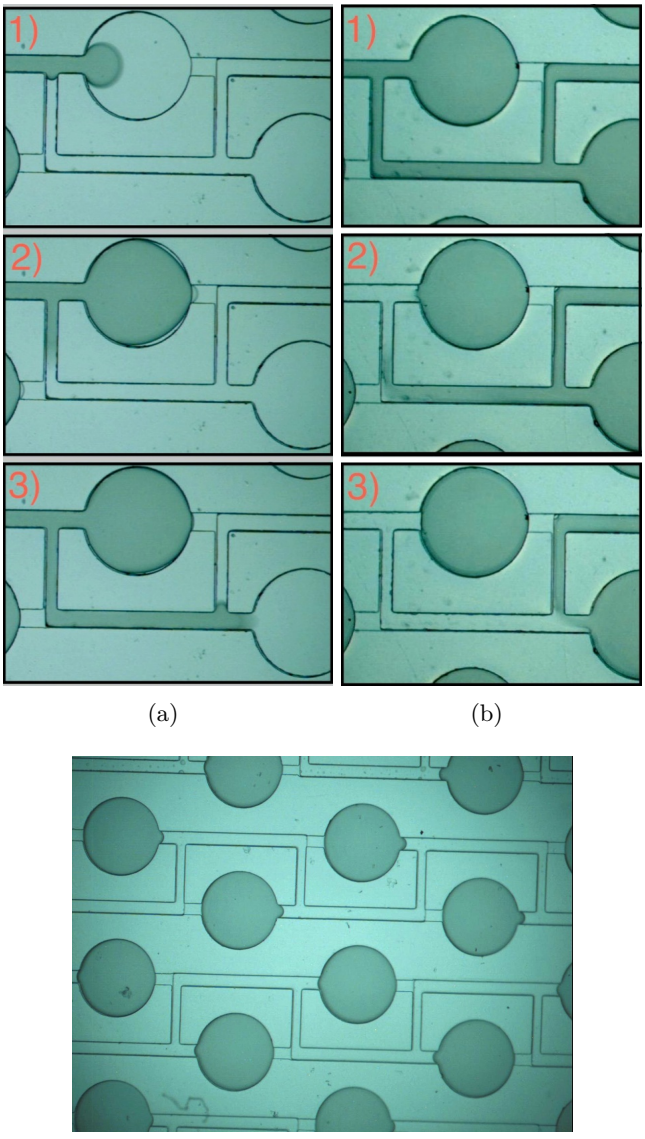

(a) (b)

(c)

Figure 4.4: *Loading the storage layer with myoglobin: (a) The sample solution enters and fills the storage well completely before flowing to the next storage well. (b) Incoming oil seals the samples in the wells. (c) 288 individual samples were produced.*

4.2 Gradient Generation in the Reservoir

The modular phase chip design allows to choose between a constant reservoir and a gradient reservoir. Both designs are described below.

In the gradient reservoir, two inlets feed the *mixing tree*, followed by the *gradient section* and the outlet. Many short serpentine channels (*diffusion zones*) in the mixing tree maximize the path of two coflowing solutions to enhance diffusive mixing. The *gradient section* consists of 12 parallel channels that are located under the storage wells in the assembled phase chip. They can provide a linear 12-step gradient from the two solutions entering the inlets. One outlet allows waste solution to exit the system.

The constant reservoir has no mixing tree and only one inlet and outlet each to provide constant conditions to all samples.

Both designs are illustrated in Figure 4.5.

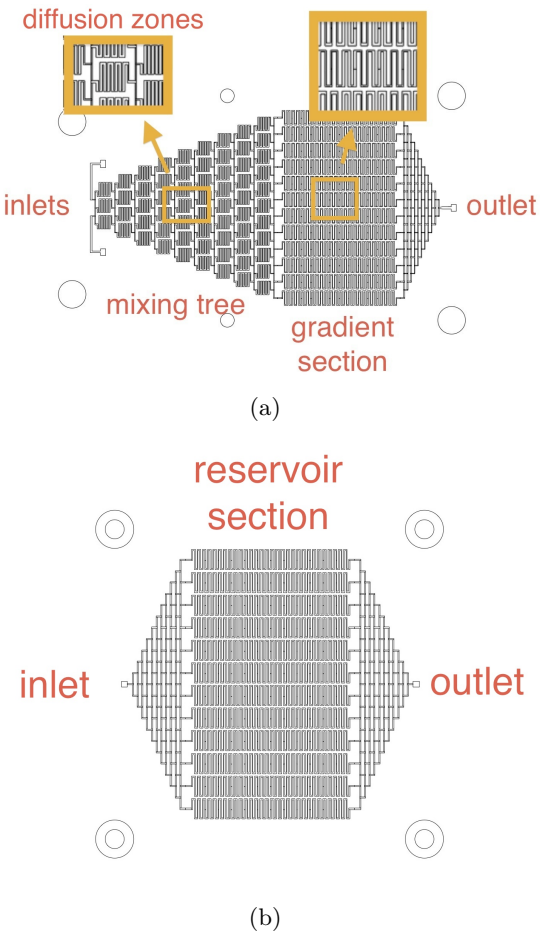

Figure 4.5: *Designs of the two different reservoirs: (a) Gradient reservoir: Two different solutions enter the channel-system and flow through the mixing tree, where they can mix diffusively. A linear distribution from the two solutions will form across the parallel channels in the* gradient section. *(b) The constant reservoir does not have a mixing tree. There is only one inlet and one outlet. All channels in the* reservoir section *carry the same solution.*

5 Characterizing the Chip

To use the phase chip for protein crystallization, it is necessary to be able to control the size of the sample droplets, since this means controlling the supersaturation of the protein. In the following experiments, water transport fluxes across the dialysis membrane were characterized as a function of hydrostatic and osmotic pressures.

When observing the sample droplets under a microscope, one can see their circumference. The height of the droplet is confined to a constant value by the height of the storage well and therefore the circumference seen in the images represents the volume of the droplets. When referring to the size of droplets in the following sections, the circumference is meant.

5.1 Water Transport Fluxes as a Function of Hydrostatic Pressures with Blocked Outlets

In this experiment, water transport fluxes through the membrane were determined as a function of hydrostatic pressures.

Setup: The chip was assembled and loaded with destilled water, the constant reservoir was filled with destilled water as well to eliminate osmotic stresses. A microfluidic channel is a hydrodynamic resistor and hence a flow will cause a pressure drop in it along the flow direction. To avoid pressure gradients within the layers, the outlets of both layers were blocked by PDMS connectors and plugs (Figure 10.10) to inhibit fluxes in the channels. A simple setup as shown in Figure 5.1 was used to apply hydrostatic pressures on the storage layer and the reservoir layer. Two vials, filled with FC-43 oil and water were mounted on a stand and connected to the storage layer and the reservoir layer by tubings. The height of the vials could be varied.

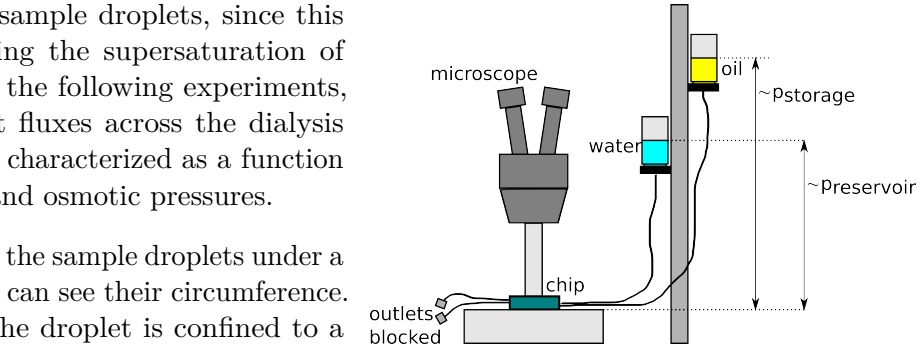

Figure 5.1: *Setup to apply hydrostatic pressures on the phase chip: Two vials, filled with FC-43 oil and water were mounted on a stand and connected to the storage layer and the reservoir layer by tubings. The height of the vials could be varied in order to apply different pressure conditions.*

Experiment: Different combinations of hydrostatic pressures were applied to the chip. Timelapses were taken to capture the kinetics of the size of the droplets for every single combination of pressures. Given that the outlets were blocked, it was assumed that all drops had equal pressure conditions and thus behaved in the same manner. Due to limited resolution of the camera, the images were taken from a part in the middle of the sample matrix. 21 different experiments were performed in total.

Evaluation: Depending on the applied pressure, the drops grew or shrunk with time. To quantify this behavior, a piece of Matlab code was written (described in Section 10.7) that was able to map the size of each individual drop in the time lapse images by recognition of the moving circumference. The code generated one plot per

drop, revealing its area over time, based on the runtime of the individual experiment. Since all curves appeared to be linear in time, a linear fit function was added to the code which allowed to extract the rates of growth of every individual drop. 11 wells were evaluated in total from each of the 21 experiments. The mean value of all rates obtained from one experiment was calculated, including the standard deviation. These rates were then normalized to the "*percentage of the total area of the storage well by that a drop would shrink within one hour*": If, for example, the rate is calculated to be "-10 % of total well area per hour" this means that within one hour the drop shrunk by the area of a tenth of the total area of a storage well, or, a completely filled storage well would be empty after 10 hours at this rate. This unit is easy to grasp and it also allows a comparison of experiments captured at different scale factors. A summary of the data can be found in Table 5.2.

The 21 rates of growth were then fit to a plane of the type

$$f(p_{storage}, p_{reservoir}) = a \cdot p_{storage} + b \cdot p_{reservoir} + c, \qquad (20)$$

resulting in the parameters shown in Table 5.1.

The results are visualized in Figure 5.2, a summary of the data can be found in Table 5.2.

Table 5.1: *Fit parameters, describing transport fluxes of water through the membrane as a function of hydrostatic pressure with blocked outlets. Units of a and b are* "percentage of total area of the storage well per hour per psi"*, the unit of c is* "percentage of total area of the storage well per hour"*.*

$a = -8.263 \pm 0.192$ (2.328%)
$b = 4.414 \pm 0.106$ (2.402%)
$c = -0.341 \pm 0.067$ (19.85%)

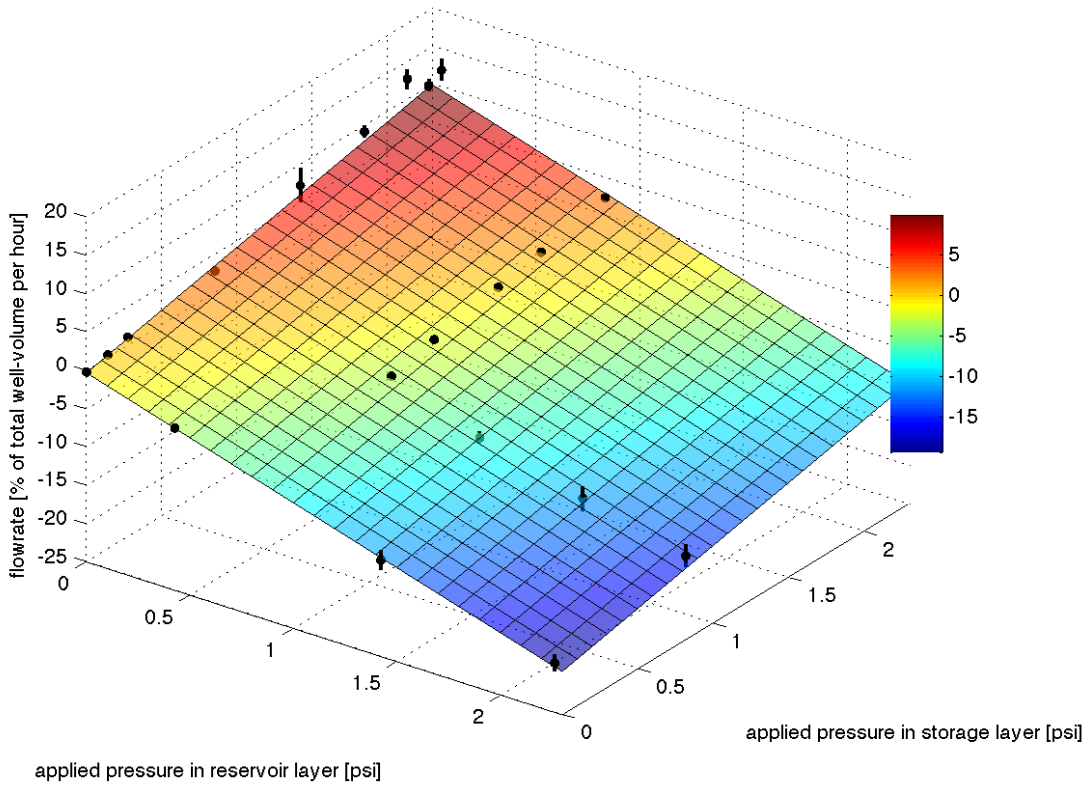

Figure 5.2: *Visualized transport fluxes of water as a function of hydrostatic pressure with blocked outlets. The plane was plotted from the data in Table 5.1. The experimental data is represented by the black dots and can be found in Table 5.2.*

Table 5.2: *Summary of the experimental data: Transport fluxes of water through the membrane measured as a function of different hydrostatic pressures with blocked outlets.*

exp #	$p_{storage}[psi]$	$p_{reservoir}[psi]$	duration of exp [s]	growth rate [% of total well area/ hour]
1	1.423 ± 0.003	0.000 ± 0.003	21660	-12.41 ± 1.32
2	0.000 ± 0.003	1.423 ± 0.003	17700	7.12 ± 2.27
3	0.000 ± 0.003	0.142 ± 0.003	54300	0.32 ± 0.13
4	0.427 ± 0.003	0.000 ± 0.003	38460	-3.83 ± 0.48
5	-0.004 ± 0.003	0.280 ± 0.003	146160	0.93 ± 0.06
6	2.270 ± 0.003	-0.007 ± 0.003	9180	-18.44 ± 1.10
7	0.854 ± 0.003	2.277 ± 0.003	54480	2.72 ± 0.10
8	0.854 ± 0.003	1.138 ± 0.003	62760	-2.17 ± 0.26
9	0.854 ± 0.003	1.565 ± 0.003	80760	-0.45 ± 0.10
10	0.854 ± 0.003	1.850 ± 0.003	89160	0.72 ± 0.08
11	2.277 ± 0.003	0.854 ± 0.003	9360	-14.65 ± 1.47
12	0.000 ± 0.003	2.277 ± 0.003	16440	9.94 ± 0.79
13	1.281 ± 0.003	0.854 ± 0.003	16020	-7.90 ± 0.80
14	0.000 ± 0.003	2.362 ± 0.003	14700	11.06 ± 1.53
15	0.000 ± 0.003	0.854 ± 0.003	57660	2.75 ± 0.20
16	0.854 ± 0.003	0.854 ± 0.003	76080	-3.56 ± 0.28
17	0.000 ± 0.003	2.135 ± 0.003	9720	12.52 ± 1.39
18	1.779 ± 0.003	0.854 ± 0.003	7680	-11.49 ± 1.63
19	0.000 ± 0.003	1.850 ± 0.003	12780	9.03 ± 0.82
20	0.000 ± 0.003	0.000 ± 0.003	59100	-0.23 ± 0.14
21	2.277 ± 0.003	2.277 ± 0.003	11460	-9.62 ± 0.43

24

Discussion: The offset plane is a good fit for the measured flux rates, since the relative errors of the fit parameters are below 3% for a and b and below 20% for c. The parameter c represents the growth rate of the droplets at pressures of zero. c is a negative number, meaning that the droplets shrink when no pressures are applied. This corresponds to the experiment (Table 5.2, exp # 20).

The parameter a represents the effect of a hydrostatic pressure in the storage layer on the growth rate of the droplets: a is negative which means that any pressure above zero results in a shrinking force for the droplets. b is positive and represents the effect of increasing reservoir pressure on the growth rate respectively: A hydrostatic pressure applied to the reservoir causes a growing force for the droplets. This observation can be explained from the principle of reverse osmosis.

Dividing a by b yields a ratio of $\frac{a}{b} = -1.9$. This means that it is easier to shrink the drops than to grow them: At the same absolute growth rates, 1.9 times more pressure is needed for growing the drops compared to shrinking them. Different values for a and b also mean that the growth rate is not only dependent on the pressure difference, but also on the absolute pressures. All these observations from the fit plane comply with the experimental observations.

5.1.1 Modelling Water Fluxes Using a Resistive Network

To explain the observed behavior, one can take advantage of the analogy between electrodynamics and hydrodynamics and model the chip with an electric network as shown in Figure 5.3.

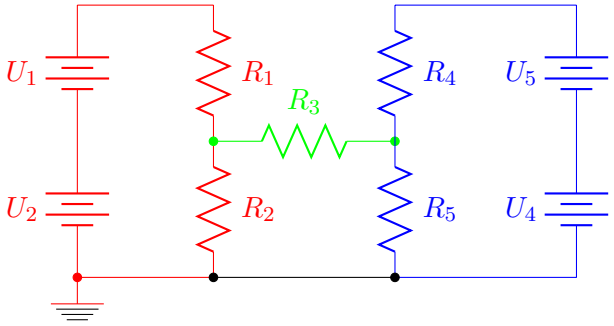

Figure 5.3: *Resistive network as a model for the phase chip: Red branch represents the storage layer, blue branch represents the reservoir layer. R_2 and R_5 model leaks while R_1 and R_4 are the respective hydrodynamic resistances of the microfluidic channels of the storage layer and the reservoir. R_3 couples both branches and is the substitute for the membrane. Any current through R_3 has to be understood as flux of water across the membrane that changes the drop size.*

The oil vial and the water vial are sources of constant pressure and can be modeled as sources of constant voltage U_1 and U_3. If there were no leaks in the chip, continuity would imply that if a volume of water enters the chip through the reservoir inlet and causes the drops to grow, the same volume of oil has to be displaced in the storage layer and to exit the chip. At blocked outlets, the displaced oil has to to exit through the inlet of the storage layer. To verify continuity, a simple experiment was performed:

Two little colored indicator drops were positioned within the inlet tubings of the storage layer and the reservoir layer. If continuity was satisfied, both drops should have moved at the same velocities, one towards the chip and the other coming from the chip. It was found that there was a discrepancy by a

factor of 30 in their velocities, so continuity was clearly not satisfied. We conclude that there must be a leak in the system. The leak could be either in the storage layer or the reservoir layer, or in both.

According to Section 3.7, the channels in both layers have flow resistances, modeled by R_1 and R_4 for the storage- and the reservoir layer. The respective leaks are represented by R_2 and R_5. These two branches are coupled by the membrane which is R_3 in the model. Any current passing through R_3 has to be understood as flux of water out of or into the drops, depending on the sign.

To solve the system, both branches have to be connected to a common ground. Two more constant voltage sources U_2 and U_4 were added. These sources form potentials that cause both, the water and the oil to evaporate from the chip. They might be related to the solubility of oil or water into the environmental air as well as the flux of water through PDMS by diffusion. Hence, the voltages of these sources depend on the temperature as well as on the oil and water saturation of the surrounding air.

We can derive three equations from the circuit according to Kirchhoff's Law:

$$-U_2 - U_1 + I_1 R_1 + R_2(I_1 - I_2) = 0 \quad (21)$$

$$R_2(I_2 - I_1) + R_2 I_2 + R_4(I_2 - I_3) = 0 \quad (22)$$

$$U_3 + U_4 + R_4(I_3 - I_2) + R_5 I_3 = 0 \quad (23)$$

A Gauss elimination yields the following equation for the current I_3, representing the flow-rate of water through the membrane:

$$I_3 = \frac{\begin{array}{l} R_2(U_1 + U_2)(R_4 + R_5) + \ldots \\ R_4(R_1 + R_2)(U_3 + U_4) \end{array}}{\begin{array}{l} (R_4 + R_5)((R_1 + R_2)(R_2 + \ldots \\ R_3 + R_4) - R_2^2) + R_4^2(R_1 + R_2) \end{array}} \quad (24)$$

In this equation, U_1 and U_3 are variables, while the constant parameters R_1 through R_5, U_2 and U_4 define the system. Since the fit plane is defined by three degrees of freedom, I_3 is overdefined by 4 variables. However, from Equation 24 we can see that this resistive network model also yields a plane because I_3 can be brought to the form

$$I_3 = A \cdot (U_1 + U_2) + B \cdot (U_3 + U_4) \quad (25)$$

$$= A \cdot U_1 + B \cdot U_3 + C. \quad (26)$$

We can see that when varying U_1 or U_3, there are two different slopes A and B in I_3. Constant U_2 and U_4 add the offset C to I_3, which corresponds to the fit parameter c.

This offset at zero of the fit plane might not only be controlled by the evaporation of water or oil. Also the Laplace pressure inside the droplets could contribute to this offset. Its influence is very small compared to the evaporation. Laplace pressure depends on the main radii of curvature of the droplets. In the storage layer, the drops are confined to the height of the storage wells. Assuming that the drops are circular, the Laplace pressure is related to their circumference as well as to their height. When the drops shrink, their height remains constant but their circumference changes causing a higher Laplace pressure in smaller drops compared

to bigger ones. Thus, smaller drops should shrink more quickly than bigger drops and their area over time plot would not be linear. As already mentioned, these curves were linear. It is therefore assumed that the Laplace pressure is negligible.

5.2 Water Transport Fluxes as a Function of Hydrostatic Pressures with Opened Reservoir Layer Outlet

In the application of the chip, the outlet of the storage layer has to be blocked. An excessive flux of oil inside the storage layer would flush the samples out of the wells in the worst case. To refresh the reservoir solution continuously, the reservoir outlet needs to be open. In the following experiment, water transport fluxes through the membrane were measured as a function of hydrostatic pressures, with open reservoir outlet.

Experiment: Different sets of pressures were applied to the chip as in the previous experiment. A similar behavior to the previous experiment was expected, but with a slight variation: Flux in the reservoir channels causes a pressure gradient along them. According to the previous experiment, this should yield a gradient in the growth rates of the droplets along the rows of the matrix. Since the channel cross-sections in the in- and outlets of the reservoir are, compared to the gradient section, smaller by a factor of 12, this variation is expected to be small. A microscope with a scanning stage was used to capture the droplets, allowing to compare the rates of different regions of the storage matrix. The different sets of applied pressures can be found in Table 5.4.

Evaluation: As expected, the drops grew or shrunk over time. The scanner divided the storage matrix into 8 x 8 images. To avoid systematic errors, droplets from the middle, the top and the bottom row in the matrix were selected, such that the mean rate of these three regions does not include the variation caused by pressure drop. The scanner took ca. 5 minutes per scan, resulting in a poor time resolution of the images that was not sufficient to run the Matlab code for the analysis. Thus, the droplet sizes had to be evaluated manually with the help of imageJ, assuming that the rates were constant in time as in the previous experiments: The areas of the droplets at the beginning and at the end of the experiments were measured and the growth rate for every individual drop was determined. These values were then processed similarly as in the previous experiment, yielding a similar plane with fit parameters in Table 5.3. The data is summarized in Table 5.4 and included in a plot of the fit-plane in Figure 5.4.

Table 5.3: *Fit parameters, describing transport fluxes of water through the membrane as a function of hydrostatic pressure with open reservoir outlet. Units of a and b are* "percentage of total area of the storage well per hour per psi"*, the unit of c is* "percentage of total area of the storage well per hour"

$a = -6.854 \pm 0.163$ (2.371%)
$b = 2.645 \pm 0.1856$ (7.016%)
$c = -0.030 \pm 0.237$ (785.3%)

Discussion: The above mentioned variation in the rates of growth was such small that it could not be quantified with imageJ. A higher pressure applied to the reservoir would increase the flux inside and thus cause

a bigger pressure drop, making this quantification easier. This "growth rate gradient" could be utilized when mapping dynamic phase diagrams: It might be possible to map different rates of increasing/decreasing protein and/or polymer concentration in the rows of the matrix versus a pH gradient provided to the columns of the matrix.

Table 5.4: *Summary of the experimental data: Transport fluxes of water through the membrane measured as a function of hydrostatic pressure with open reservoir outlet*

exp #	$p_{storage}[psi]$	$p_{reservoir}[psi]$	duration of exp [s]	growth rate [% of total well area/ hour]
1	1.992 ± 0.003	0.248 ± 0.003	23100	-12.57 ± 0.85
2	0.000 ± 0.003	1.992 ± 0.003	51600	5.20 ± 0.62
3	0.996 ± 0.003	0.996 ± 0.003	21420	-4.14 ± 0.60
4	1.992 ± 0.003	1.992 ± 0.003	21720	-8.51 ± 0.39
5	0.000 ± 0.003	0.996 ± 0.003	65820	3.04 ± 0.64
6	0.000 ± 0.003	-0.000 ± 0.003	87060	-0.30 ± 0.50

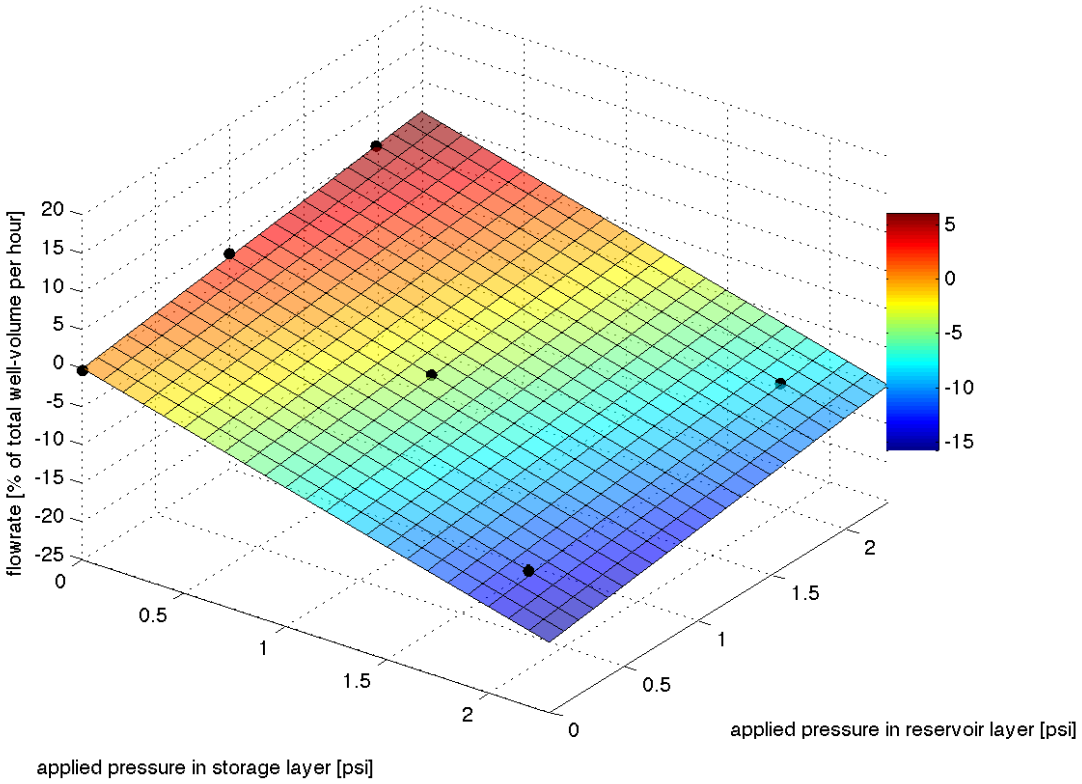

Figure 5.4: *Visualized transport fluxes of water through the membrane as a function of hydrostatic pressures with open reservoir outlet. The plane was plotted from the data in Table 5.3. The experimental data is represented by the black dots and can be found in Table 5.4.*

5.3 Water Transport Fluxes as a Function of Hydrostatic Pressure in Storage Layer and Flow-rate in Flow-Driven Reservoir Layer

Setup: The same setup as in the previous experiments was used, but the reservoir layer was unplugged from the vial and connected to a syringe pump to be driven by constant flux. Its outlet remained open.

Experiment: Water transport fluxes through the membrane were determined as a function of hydrostatic pressures applied on the storage layer and the flow-rate in flow-driven reservoir.

Evaluation: The experiments were again analyzed manually with imageJ as described in the previous experiment and yield the typical linear plane with the fit parameters in Table 5.5.

Table 5.5: *Fit parameters describing transport fluxes of water through the membrane as a function of hydrostatic pressure in storage layer and the flow-rate in flow-driven reservoir layer with open reservoir outlet: The unit of a is* "percentage of total area of the storage well per hour per psi"*, the unit of b is* "percentage of total area of the storage well per $[\mu l/hr]$"*, the unit of c is* "percentage of total area of the storage well per hour"

$a = -7.283 \pm 0.163$ (5.239%)
$b = 0.069 \pm 0.021$ (30.88%)
$c = -0.421 \pm 0.976$ (231.8%).

The experimental data can be found in Table 5.6 and the corresponding plot of the fit plane and the data is shown in Figure 5.5.

In principle, a pump could be used to refresh the reservoir continuously. Nevertheless, there is a risk that an excessive pressure

Table 5.6: *Summary of the experimental data: Transport fluxes of water through the membrane measured as a function of hydrostatic pressure in the storage layer and the flow-rate in flow-driven reservoir layer with open outlet*

exp #	$p_{storage}[psi]$	$flow-rate_{water}[\mu l/h]$	duration of exp [s]	growth rate [% of total well area/ hour]
1	1.992 ± 0.003	30	23100	–13.07 ± 1.24
2	0.000 ± 0.003	30	51600	1.72 ± 0.81
3	1.992 ± 0.003	60	21420	-8.86 ± 3.91
4	0.000 ± 0.003	60	21720	3.59 ± 0.90

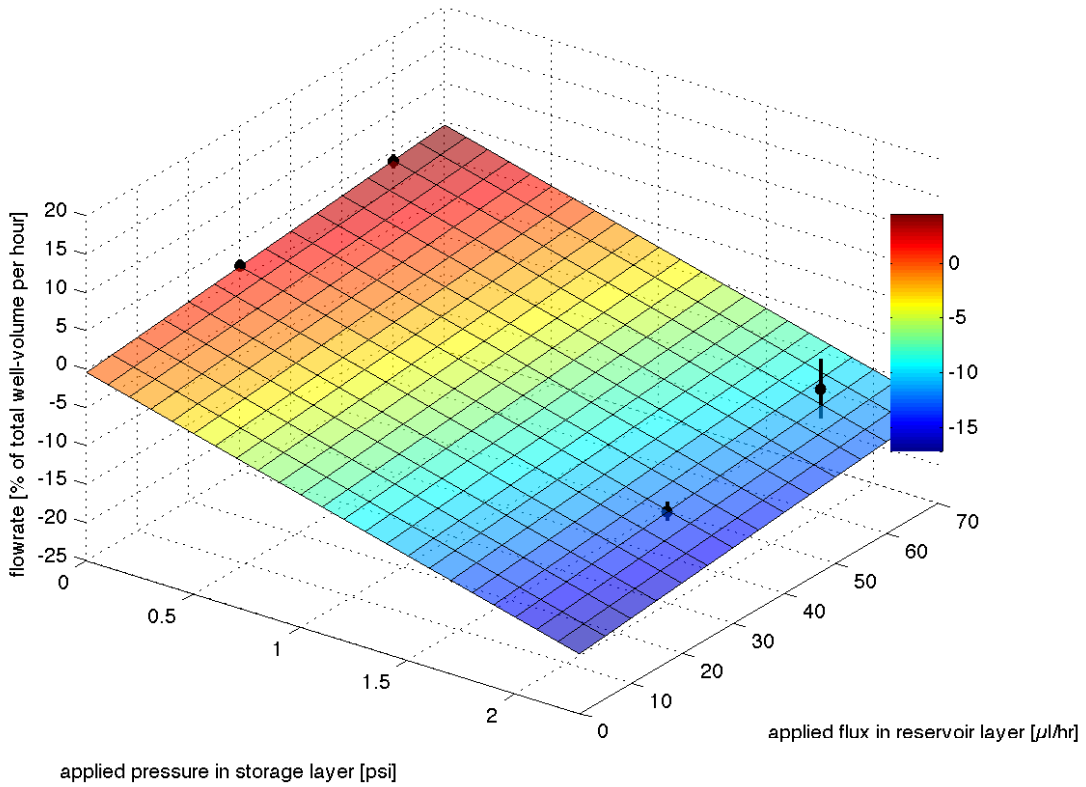

Figure 5.5: *Visualized transport fluxes of water through the membrane as a function of hydrostatic pressure in storage layer and flow-rate in flow-driven reservoir with open reservoir outlet. The plane was plotted from the data in Table 5.5. The experimental data is represented by the black dots and can be found in Table 5.6.*

can build up caused by partial clogging of channels from small particles, etc.. This actually happened in one of the experiments: After a couple of hours of shrinking, the droplets started to grow excessively. It is suggested to operate the chip fully at constant pressures.

5.4 Controlling the Droplet Size by Combining Osmosis and Reverse Osmosis

Manipulation of the droplet size is not sufficient for a reliable and reproducable operation of the phase chip. Their size has to be controlled, because this means controlling protein and/ or precipitant concentration and thus supersaturation. This can be achieved by combining osmosis and reverse osmosis:

If there is an osmotic pressure that causes the droplets to grow by drawing water from the reservoir, a hydrostatic pressure can be applied on the storage layer, that matches the osmotic pressure of the droplets or even lies above. In the last named case, water would be forced into the reservoir by reverse osmosis, while the osmolarity in the droplets increases. After a while, the droplets should reach a stable equilibrium, where osmosis and reverse osmosis stabilize the drop at a certain size and osmolarity.

The pressure drop in the reservoir layer that was discussed in Section 5.2 can also be applied here: It would allow different stationary states in the columns of the matrix.

Membranes of different molecular weight cut-off can be incorporated, depending on the desired experiment:

- When using a membrane of a molecular cut-off below the polymer size, both the protein and the polymer remain in the droplets and their partial pressures add. Countering the total osmotic pressure by reverse osmosis allows to control the protein and polymer concentration while their relative concentration remains constant.
- A membrane of a high molecular weight cut-off also allows the polymer to diffuse through, but not the protein. The total osmotic pressure in this case is equal to the partial pressure of the protein. A variation of the droplet size varies the protein concentration while the polymer concentration is constant. This is not possible in conventional crystallization methods.

Experiment: To verify this functionality, droplets of a 10 w % solution of PEG 8000 were loaded and the reservoir was filled with the same solution to inhibit initial osmotic stresses. The reservoir layer (constant reservoir) was connected to a syringe pump for constant flux. Its outlet was open in order to refresh the PEG solution continuously to keep the concentration at the same initial value. The reservoir was driven at $30\mu l/hr$ and the end of its outlet tubing was inserted through a small hole into the lid of a vial to prevent clogging from precipitation of the PEG. A pressure of $1.992 \pm 0.003 psi$ was applied on the storage layer. The same experiment was performed with membranes of 1.5 and 7.5 kD molecular weight cut-off.

Results: In theory, applying a hydrostatic pressure on the storage layer in this case would slightly decrease the size of the droplets, yielding a stationary state where the excess osmotic pressure balances the hydrostatic pressure, or where osmosis balances reverse osmosis. The droplets shrunk in both cases until all storage wells were empty. There

was no precipitant left in the storage wells, indicating that the PEG must have left the storage wells, even at low molecular weight cut-off. To verify this assumption, flourescently labeled polymer could be used to observe, if it vanishes from the storage wells. There is possibly enough space between the membrane and the Teflon foil for the polymer to leave the chip: The Teflon foil and the surface of the storage well are hydrophobic and hence the droplet can only connect to the membrane. The membrane and the foil are kept in place and sealed only by the contact pressure provided by screws that hold all layers together. The Teflon foil is very thin ($25\mu m$) and might slightly invaginate into the channels of the storage layer, yielding very narrow channels between the membrane and the Teflon foil that cause the leak.

5.5 Conclusion

An understanding for the reverse osmotic behavior of the phase chip was obtained from the experiments. The results can be applied to manually balance the size of the droplets by applying pressure conditions that yield a growth rate at zero. It was proven that there is a leak in the chip which has to be minimized in future designs. It might be possible to create a seal from PDMS, that encloses the membrane and the microfluidic channels like a gasket.

So far, the droplets could not be stabilized by combining osmosis and reverse osmosis, although this is necessary for a reliable and reproducable operation of the phase chip. Once there is a technique that allows to bond the Teflon sheet to the membrane to prevent this leak, this feature should be feasible. The tricky part is to manage the fact that the membrane swells or shrinks depending on its wetness: The Teflon sheet as well as the bond would have to be flexible and yet durable. The Teflon has to adhere to the membrane even when it is wet. A Teflon silicone based adhesive tape was attached to a dry membrane. As soon as the membrane was wet, it swelled causing the sandwich to curl like a bimetal. After a while, the teflon tape came off. Thus, a Teflon adhesive tape is not an option to inhibit this leak.

6 Characterization of the Gradient Reservoir

In this section, the proper function of the gradient reservoir was tested using constant flux and constant pressure as driving forces. The effect of viscosity on the function was examined and the flow resistance of the gradient reservoir was measured. Based on that, an example is given to estimate the maximum flowrate that ensures proper gradient formation, depending on the diffusion constant of the solutions used.

The gradient reservoir by itself was plasma bonded to a glass cover slide to seal the channel network and to allow the operation without external influences.

6.1 Generating a Gradient from Solutions of Different Viscosities

6.1.1 Flow Driven

Experiment: It was attempted to generate a linear gradient of PEG concentration. Two syringes were filled with blue colored water and a red colored solution of 10 w% PEG 8000. Food dye was used as a color in both cases. Two syringe pumps were equipped with the syringes and connected to the reservoir inlets. The flow-rates were set to $30\mu l/h$.

Evaluation: After a few minutes, a good distribution from blue to red seemed to appear in the gradient section of the reservoir. Only a closer look revealed that the gradient formation did not work properly. Since the viscosity of the PEG solution is much higher than the viscosity of pure water, the PEG occupied more channel cross-section within the mixing tree and the gradient section.

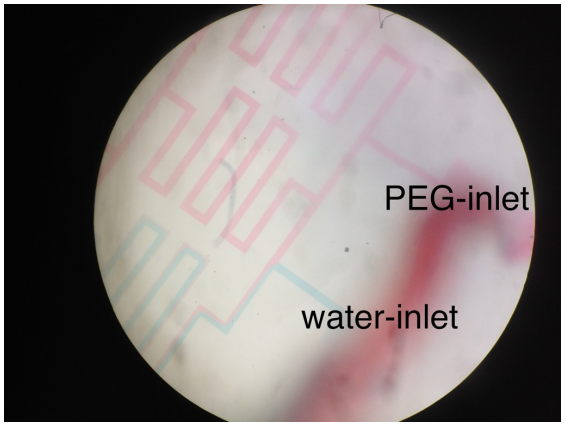

Figure 6.1: *Producing a gradient from solutions of different viscosities at constant flux: The red PEG solution is more viscous and occupies more channel cross-section within the mixing tree (and the gradient section). The mixing thus does not work properly and a linear gradient can not be produced.*

The microscope reveals this more clearly in Figure 6.1.

We can explain this behavior using Hagen Poiseuille's law. Both liquids flow through parts of the channel network. We can consider the parts of the network occupied by the red and the blue solution as separate, fictive channels, that have different geometries and thus different flow resitances C_{red} and C_{blue}. The flow-rates in both inlets are equal:

$$I_{red} = I_{blue} \tag{27}$$

$$\Rightarrow C_{red} \cdot \frac{p_{red}}{\eta_{red}} = C_{blue} \cdot \frac{p_{blue}}{\eta_{blue}} \tag{28}$$

Any pressure differences perpendicular to the flow direction balance, yielding $p_{red} = p_{blue}$. η_{red} and η_{blue} represent the viscosities of the two liquids. Since $\eta_{red} > \eta_{blue}$, only $C_{red} < C_{blue}$ can satisfy Equation 28, which is the experimental observation.

$C_{red} = C_{blue}$ is the condition for proper function of the gradient because this means that both solutions occupy equal fractions of the channel network. It is not possible to generate a linear gradient from two solutions of different viscosities, since Equation 28 can not be satisfied with $\eta_{red} > \eta_{blue}$ and $C_{red} = C_{blue}$.

6.1.2 Pressure Driven

Constant flux ensures that the fractions of the channels that are occupied by the red and the blue solution respectively are constant in time. At constant pressure, these fractions may change and thus a pressure driven gradient of solutions of different viscosities has proven to be highly instable. It is not possible to operate the gradient layer solutions of different viscosities, especially not if driven by constant pressures.

6.2 Generating a Gradient of Solutions of Matched Viscosities, Pressure Driven

Experiment: The same experiment as in Section 6.1 was performend using two liquids with matched viscosities. Two vials were mounted on a stand and connected to the the gradient reservoir by tubings. The height of the vials could be varied, but they were always kept at the same height to have equal flow-rates for both solutions ($I_{red} = I_{blue}$). Solutions of 25 w% PEG 4000 colored with food dye were used. Both pressures were set to the same values of $0.427 \pm 0.0028 psi$. The setup is shown in Figure 6.2. Images were taken regularly during a period of 3 days.

Results: At matched viscosities, the gradient has proven to be stable. The color distribution did not change observably over 72 hours as shown in Figure 6.3.

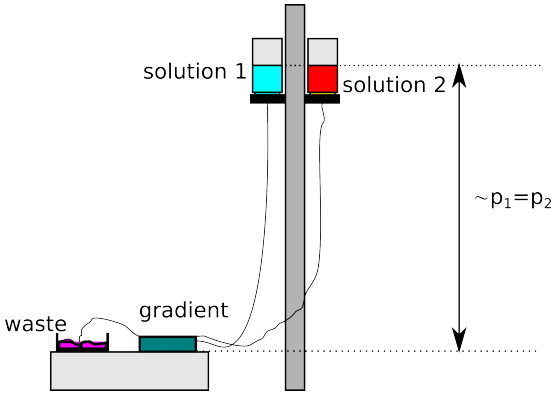

Figure 6.2: *Setup to drive the gradient reservoir by hydrostatic pressures: Two vials filled with solutions of matched viscosities were mounted on a stand and connected to the the reservoir layer by tubings. The height of the vials could be varied, but they were kept at the same height during the experiments to have equal flow-rates for both solutions.*

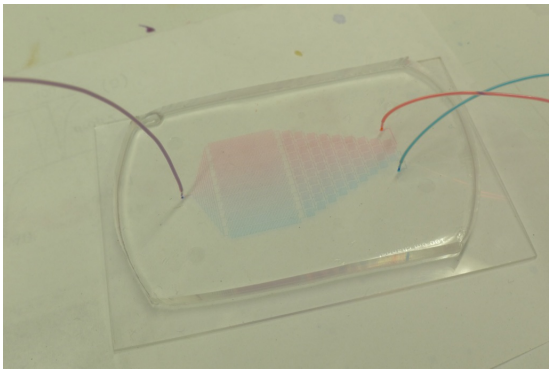

(a)

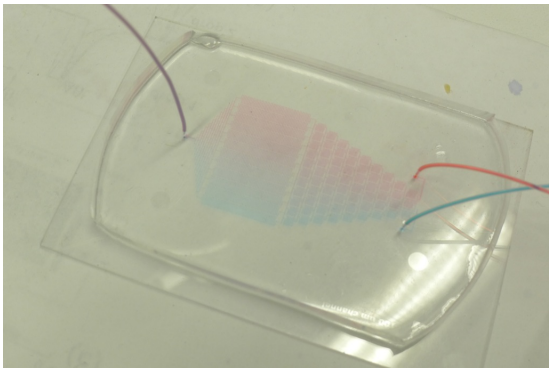

(b)

Figure 6.3: *Generating a pressure driven gradient of solutions of matched viscosities: The distribution of the colored PEG-solutions is stable: (a) Distribution after one hour (b) Distribution after 72 hours.*

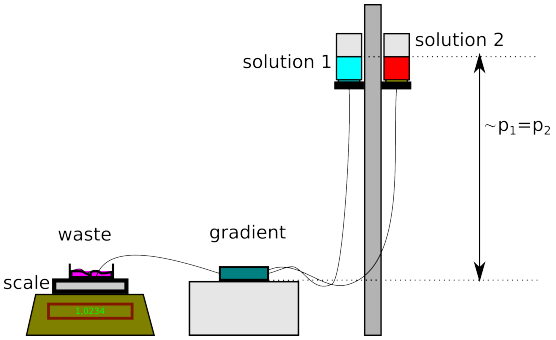

Figure 6.4: *Setup to measure the hydrodynamic resistance of the gradient reservoir: Vials containing solutions of matched viscosities were kept at the same relative height while their height from the chip was varied. Flow-rates were measured as a function of pressure and viscosity using a high precision scale.*

6.3 Characterizing the Hydrodynamic Resistance of the Gradient Reservoir

The following experiments were performed to determine the hydrodynamic resistance of the gradient reservoir. This number helps to estimate the pressure settings that are necessary for proper operation of the gradient reservoir.

Setup: As in previous experiments, two vials mounted on a stand were used to apply hydrostatic pressures on the gradient reservoir. The weight of waste solution exiting the chip per period of time was measured with a high precision scale. The setup is shown in Figure 6.4

Experiment: Throughout the experiments, the height difference between the two vials was kept at zero to obtain equal flow-rates for both viscosity-matched solutions. Different pressures were applied and the weight gain per time in the waste container was measured. The experiment was performed for solutions of 25 w% PEG 4000 colored with food dye and for water colored with food dye.

Evaluation At room temperature, a solution of 25 w% PEG has a density of 1.05 g/ml [msd], the density of water is 1.00 g/ml. This allows to convert the weight gain per time to flow-rates in units of nl/s. Assuming a flux of zero at a pressure of zero, both datasets were fitted to a simple linear equation of the type $f(p) = a \cdot p$. The fit-data can be found in Table 6.1 and a plot of the data and the fit in Figure 6.5.

Table 6.1: *Fit-parameters, describing flow-rates in the reservoir as a function of applied pressure.*

Solution	Flow-rate $\left[\frac{nl}{s \cdot psi}\right]$
water	202.11 ± 4.439
peg 4000 10w%	22.778 ± 4.414

The small standard deviation of the fit parameters indicates, that the linear model represents the data very well. As Hagen Poisseuille's Law predicts, flux in the channels is linear in pressure. The fit parameter of the water and its viscosity of $\eta = 1.002 \cdot 10^{-3} Ns/m^2$ allow to calculate C, the hydrodynamic resistance of the reservoir:

$$I =: C \cdot \frac{\Delta p}{\eta} \tag{29}$$

The fit parameter for water

$1psi \hat{=} 202nl/sec \pm 4nl/sec$ yields

$$C = \frac{I \cdot \eta}{\Delta p} = (2.94 \pm 0.06) \cdot 10^{-17} m^3 \tag{30}$$

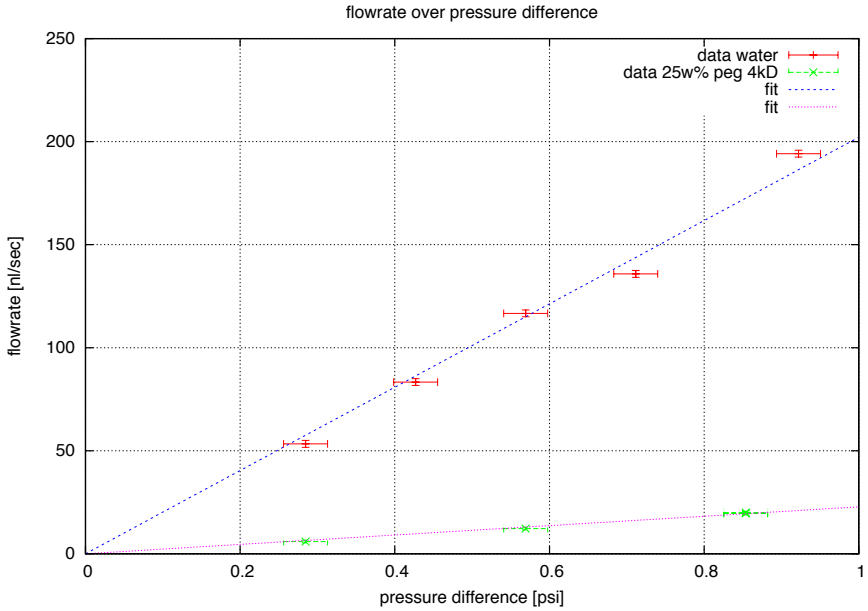

Figure 6.5: *Mesured flow-rates in the gradient reservoir as a function of the applied pressure and linear fits of the data.*

With C, it is now possible to estimate the resulting flux in the gradient reservoir depending on the driving pressure and the viscosity of the viscosity-matched solutions.

6.3.1 Estimating the Optimal Flow-Rate for a Reservoir Solution with Respect to its Diffusion Constant

The flow-rates in the gradient reservoir have to allow a critical time t_{max} that is necessary for both liquids to mix diffusively in the diffusion zones of the mixing tree. The smallest cross-sectional area in the gradient where diffusive mixing has to happen is at the beginning of the tree system, where the two inlet streams split into three channels. In this region of the reservoir, the flow-rate reaches its maximum. The total cross-sectional area of these three channels is $A = 30000\ \mu m^2$. The length of the diffusion zones was measured from the reservoir CAD file as $l = 14mm$. To calculate the optimal flow-rate, the critical time t_{max} has to be calculated:

According to the Stokes Einstein equation, the diffusion constant of spherical particles of a radius r in a liquid of the viscosity η can be calculated as

$$D = \frac{k_B T}{6\pi\eta r} \tag{31}$$

[nyu]. It is obvious that D scales inversly with the radius of the particle. An estimate for the time it takes for a particle to travel across the distance a at a diffusion constant D is given by

$$t_{max} = \frac{a^2}{2D} \tag{32}$$

[nyu]. Substitution of the Stokes Einstein relation shows that the diffusion time scales linear with the radius of the particle:

$$t_{max} = \frac{a^2 \cdot 6\pi\eta r}{2 \cdot k_B T} \tag{33}$$

As a rough estimate, the molecules of the solutions have to travel at least half of the channel width w to completely mix. With $a = \frac{w}{2} = 50\mu m$, the time t_{max} can be calculated for given T, η and r. For the value of r, the biggest hydrodynamic radius of all involved particles has to be used, since its diffusion time is the longest. The maximum allowed flowrate is with A and l:

$$I_{max} = \frac{V}{t_{max}} = \frac{A \cdot l}{t_{max}}$$

$$= \frac{300000\mu m^2 \cdot 14mm}{t_{max}}. \tag{34}$$

Applying Hagen Poiseuille's Law with C from Equation 30 will allow to estimate the maximum pressure Δp_{max} for the given viscosity η:

$$\Delta p_{max} = \frac{I_{max} \cdot \eta}{C}$$

$$= \frac{I_{max} \cdot \eta}{(2.94 \pm 0.06) \cdot 10^{-17} m^3} \tag{35}$$

With the data in Table 5.3, the storage layer pressure that balances the droplets at a reservoir pressure Δp_{max} can be calculated by setting the transportation flux $f = 0$ in the fit-plane Equation 20.

6.4 Conclusion

All the characterizations that were performed helped to get a deeper understanding on how the phase chip can be operated. The experiments helped to estimate the growth rate of the sample droplets depending on the hydrostatic pressrures that are applied. Furthermore, it was shown under which conditions the gradient reservoir works properly. Constant pressure has proven to be the best method to operate the phase chip.

7 Crystallizing Proteins in the Phase Chip/ Quality Analysis

The capability of the new chip design of producing protein crystals was tested. Glucose isomerase was used as a dummy protein.

Experiment: Two chips were set up with a constant reservoir and loaded with a 1:1 mix of a protein solution (64 mg/ml glucose isomerase and 10 mM Hepes pH 7.5) and a buffer solution (10 μl 40 w% PEG 10k, 100 mM ammonium sulfate pH 7.3). The same buffer was also flushed through the reservoir during the loading and replaced by a solution of increased 30 w% PEG afterwards. A third chip was loaded with the same protein mix without changing the reservoir solution after the loading. All chips were disconnected from the pumps after the loading, all inlet and outlet tubings were plugged and they were stored at $4°C$.

Results: After a few days, crystals appeared in the chips (Figure 7.1). The remaining liquid in the tubings was drawn into the chips, indicating that water and oil might have evaporated that yielded an increasing supersaturation.

The crystals were extracted from the chip (described in Section 10.4) and analysed in a syncrotron beam at MAC CHESS at Cornell University. The highest resolution obtained from the crystals reached 1.19 Å at a mosaicity of 0.22°. The diffraction pattern

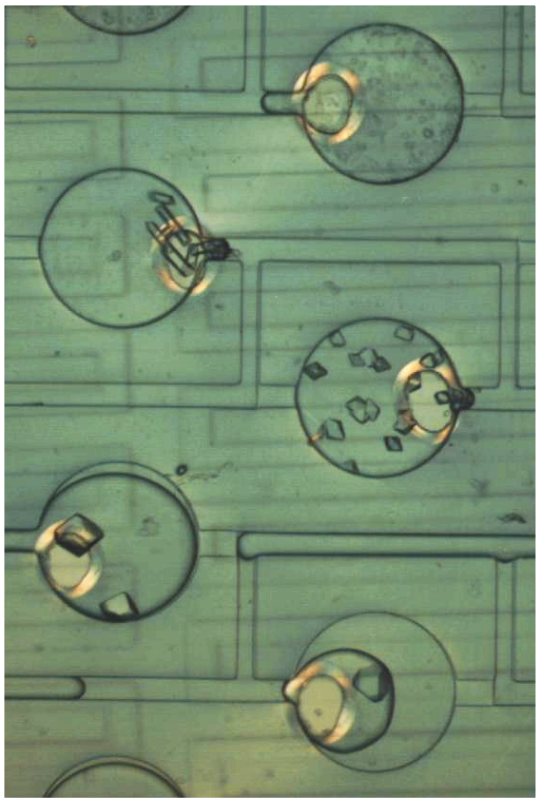

Figure 7.1: *Crystals of glucose isomerase grown in the phase chip.*

of this best crystal can be seen in Figure 7.2.

Conclusion: It was proven that proteins can be crystallized in the new dialysis phase chip at a good quality.

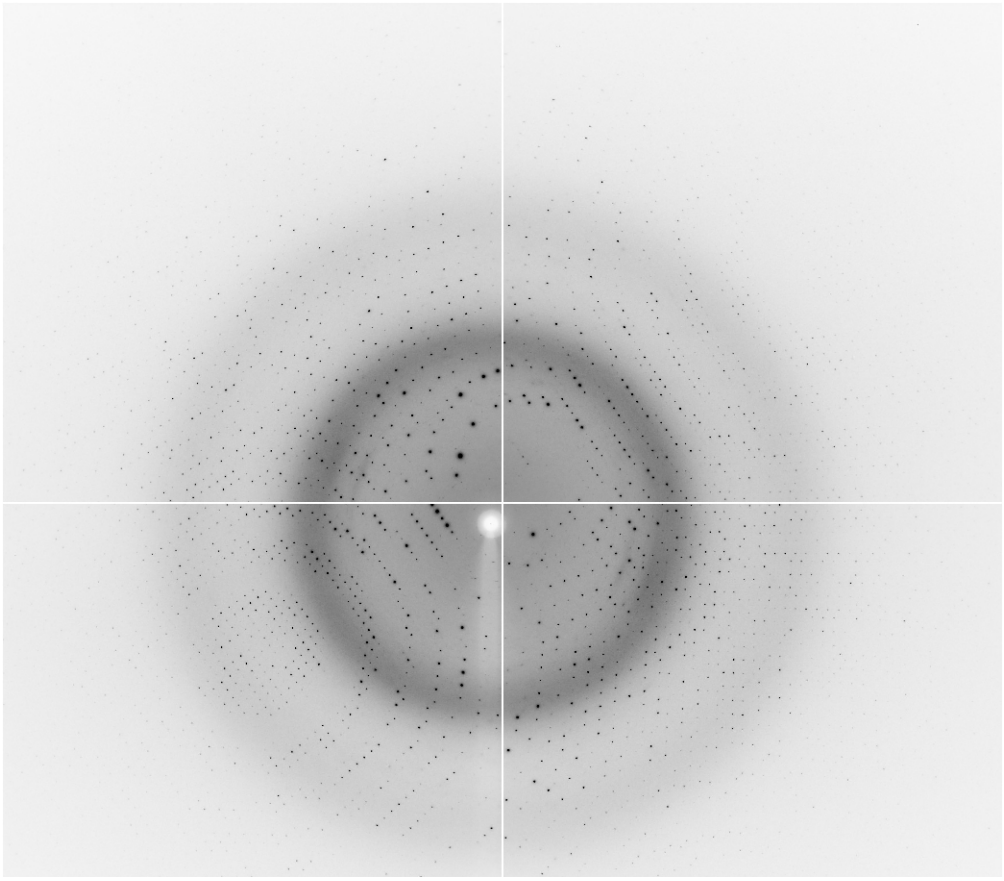

Figure 7.2: *Diffraction pattern of a glucose isomerase crystal grown in the phase chip: Diffraction to a resolution of 1.19* Å *at a mosaicity of* 0.22°.

8 Mapping a Phase Diagram of the D1D2 Heterodimer of Varying pH

Although the chip was not ready at this point to perform experiments, the results of the characterization were applied in an attempt to map a phase diagram of the D1D2 heterodimer. Together with Michael Heymann and in collaboration with Prof. Dr. Daniel Pomeranz Krummel and Kelsey Anthony from the Biochemistry Department at Brandeis University, the influence on different polymer concentrations versus pH on the crystallization of the D1D2 heterodimer was screened by the conventional sitting drop method. We found that a minimum polymer concentration of 25 w% PEG 4000 seemed to necessary to crystallize D1D2 within a week. It was attempted to map a 1-dimensional phase diagram of varying pH using the dialysis phase chip method.

Experiment: The sample of D1D2 was isolated by Michael Heymann and Kelsey Anthony. The storage solution contained the following ingredients:

- 20 mM Hepes @ pH 7.5 (238 Dalton)
- 200 mM NaCl (58 Dalton)
- D1D2 Protein $7.5 mg/ml$

Adding the partial pressures obtained from Van't Hoff's formula and neglecting the osmotic pressure of the protein results in a total osmotic pressure of:

$$p_{Proteinsolution} = 7psi + 72psi = 79psi \tag{36}$$

Two different Buffer solutions A and B of pH 5 and pH 6 were mixed from the following ingredients:

- 1 M sodium citrate (258 Dalton)
- 0.2 M ammonium acetate (77 Dalton)
- 2 M Glycerol (92 Dalton)
- 62.5 mM PEG 4000 (25 w%)

The osmotic pressures of these solutions were calculated to be

$$p_{Buffer} = 361psi + 72psi + 722psi + 22psi \tag{37}$$

$$= 1177psi, \tag{38}$$

although Van't Hoffs formula is not accurate in this high concentration regime. To minimize osmotic effects in the chip, both the protein solution and the reservoir solution should have equal osmotic pressures. A solution C of the following ingredients was mixed:

- 200 mM NaCl (58 Dalton)
- 6.26 M Glycerol (92 Dalton)
- 62.5 mM PEG 4000 (25 w%)

This solution has an osmotic pressure of

$$\begin{aligned} p_{additive} &= 72psi + 2260psi + 22psi \\ &= 2345psi \\ &\approx 2 \cdot p_{Buffer} \end{aligned} \tag{39}$$

Solution C was then mixed 1:1 with the protein solution such that the resulting solution D had the same osmotic pressure as the buffer solutions A and B. C was also mixed with water (Solution E).

The chip was then set up and prepared for loading. The reservoir was filled with solution E, solution D was loaded. The chip was transferred to a scanning stage with the

pressure driven setup used in previous experiments employing a stand and *three* vials adjustable in height. The buffer solutions A and B were filled into vials and both were set to a height equal to $0.427 \pm 0.003 psi$ in reference to the chip. From Table 5.3 and Equation 20, a hydrostatic pressure of $p_{storage} = 0.381 psi$ was calculated to be necessary to balance the droplets (growth rate equals zero). This pressure is equal to a height of 26.8 cm. The third vial was filled with oil, set to this height and the scanner was started. To prevent thickening of the viscous solutions in the reservoir from the evaporation of water, the chip was surrounded by wetted paper wipes, that were kept wet continuously by a syringe pump.

Results: There was no flux in the reservoir, although it did not seem to be clogged during the loading procedure. Even higher pressures could not force the solution through the reservoir. The experiment was aborted after 24 hours. Water might have evaporated through the gap between the layers, that results from the thickness of the membrane, thickening the reservoir solution more and more. A wet environment apparently did not prevent the evaporation of water sufficiently.

9 Conclusion

The following conclusions are drawn from all the above experiments: Constant pressure and constant flux have to be combined in the operation of the phase chip. Constant flux is needed for loading. Reverse osmotic water transport fluxes through the membrane depend linear on the pressures applied to the storage- and reservoir layer of the chip. Because of leakage fluxes, they depend on absolute pressures and not only the pressure difference applied. This makes it is easier to shrink the droplets than to grow them. When growing them, water and solutes from the reservoir solution seem to pass through the membrane from the reservoir into the droplet. When shrinking them, water and solutes from the droplet seen to pass through the membrane into the reservoir and *also* through small invaginations of the Teflon foil, causing a leak and the loss of sample material. All leaks have to be inhibited before the phase chip is applicable in its purpose. Combining osmosis and reverse osmosis is a method to control the supersaturation of the protein samples. Thus, during experiments the chip has to be driven by constant pressures for reproducable results. Constant flux would not ensure reproducable pressure conditions. For a proper gradient function, solutions of matched viscosities have to be used in the pressure driven gradient. The dialysis phase chip has proven its capability of producing protein crystals of good quality.

10 Materials and Methods

10.1 Manufacturing the Phase Chip

This section provides instructions for the manufacturing of the phase chip.

10.1.1 Manufacturing the Reservoir

List of materials for the production of a PDMS reservoir:

- Negative photomask from reservoir design
- Si-wafer
- SU8 negative photoresist (Microchem [mic])
- SU8 developper
- Isopropanol
- PDMS and crosslinker, Dow Corning, Sylgard 184
- PDMS Mixer
- Spincoater
- UV-exposure unit
- 3 hot plates (65, 95 and 180 $°C$)
- Vacuum chamber
- Oven ($70°C$)
- Scalpel
- Hole puncher, $0.75mm$ and $5mm$ diameter
- Scotch tape

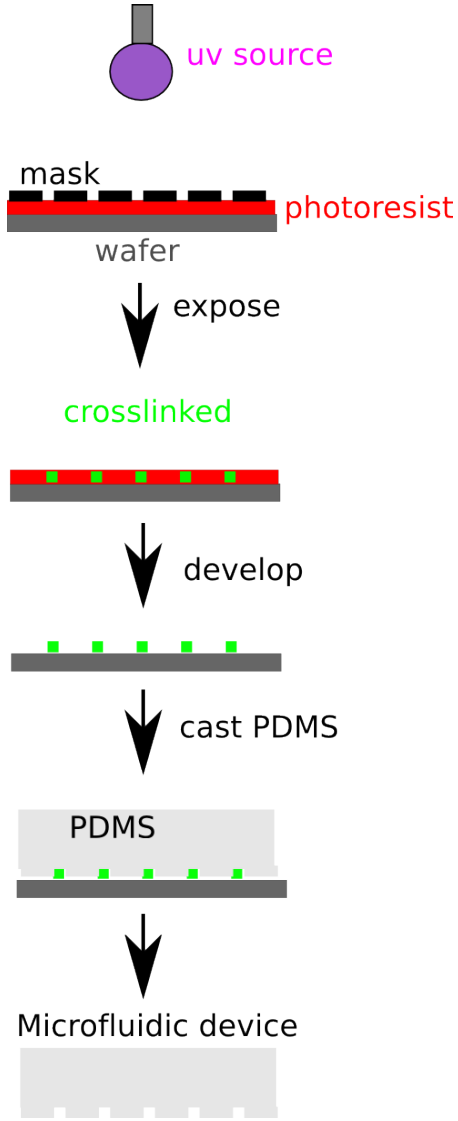

Figure 10.1: *Soft lithography process for making microfluidic devices from PDMS, reproduced from [Sel10]*

The process of making microfluidic devices from PDMS by soft lithography is explained in Figure 10.1.

All photomasks were designed in Autocad. The protocol in the SU8 datasheet [mic] was used for the fabrication of the master: A $100\mu m$ layer of photoresist is spincoated

onto a wafer, followed by a soft-bake at temperatures of 65 $°C$ (5 min) and 95 $°C$ (15 min). A cool-down is needed to solidify the photoresist. The coated wafer is placed on the UV exposure unit with the photomask arranged on top of the photoresist. A typical energy of 200 mJ/cm^2 is necessary to crosslink the 100μm layer. After the exposure, a post exposure bake at 65 $°C$ (2 min) and 95 $°C$ (8 min) has to be performed, followed by a cool-down. The developer is applied to remove the unexposed parts of the photoresist, remainders have to be rinsed with isopropanol afterwards. As a last step, the wafer has to be hard-baked at 180°C (25 min). To prevent the wafer from cracking, it is needs to be cooled down stepwise afterwards by employing all three hotplates.

The wafer can now be used to produce the PDMS reservoir: A petri dish is lined with aluminum foil to allow removing the wafer afterwards. The wafer with the features on top is placed in the petri dish (Figure 10.2). The PDMS is mixed with the crosslinker in a weight ratio of 1:10 in a mixer, which removes inhomogenities and trapped air bubbles. It can then be carefully poured onto the wafer. A vacuum chamber helps to remove trapped air bubbles from the features. All bubbles should float on the surface of the PDMS afterwards, where they can be removed carefully with scotch tape. The PDMS is cured at a temperature of 70 °C for 45 minutes and can be lifted off the master with a scalpel after cooling down. The inlet- and outlet holes and the through-holes for the screws have to be punched with the hole puncher. The reservoir is ready for use.

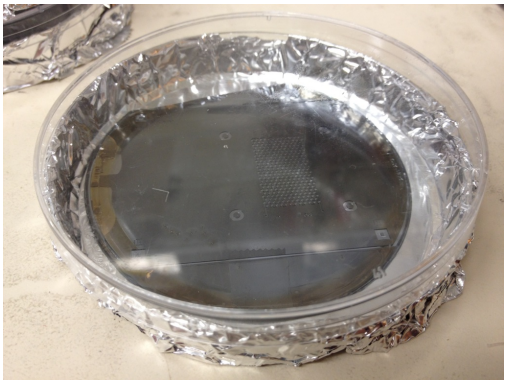

Figure 10.2: *Manufacturing the reservoir: Wafer with photoresist features in a petri dish lined with aluminum foil*

10.1.2 Manufacturing the Plexiglass Bottom Piece

Plexiglass in the thickness of 12mm has proven to be robust and stable enough for a bottom piece. Threaded holes were drilled as well as holes to run the reservoir layer tubing through the bottom plate.

10.1.3 Manufacturing the Storage Layer

List of Materials:

- All the items as listed above in the reservoir manufacturing section
- Custom plexiglass mold
- Polyurethane “crystal clear 204” from Smooth-On, Inc.
- Oven (150°C)
- Tubing, Cole Parmer PEEK, 300 μm inner diameter
- Aligner
- 1ml plastic syringe with rubber piston

The manufacturing of the storage layer is a little more extensive, since it involves a process of making a PDMS mold for casting the polyurethane storage layer (Figure 10.3 (b) & (c)).

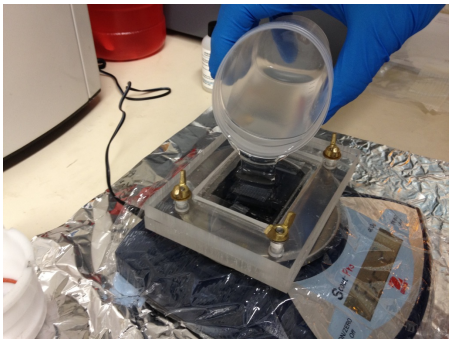

(a)

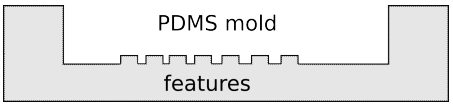

(b)

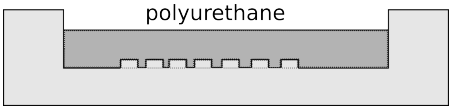

(c)

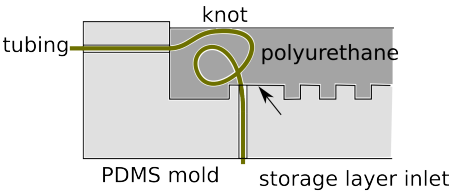

(d)

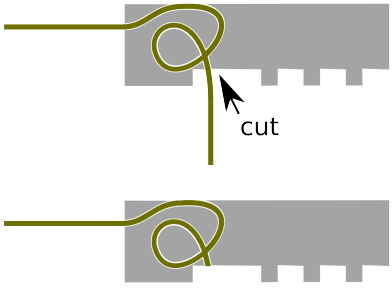

(e)

The storage layer is a double layer design. A first layer of $75\mu m$ thick SU8 is spincoated onto a wafer, soft-baked, exposed, post exposure baked. A second $25\mu m$ layer of photoresist is spincoated on top of the undeveloped first layer, followed by another soft-bake and a cool down period. By the help of the aligner, the photomask of the second layer is arranged on top such that it matches the slighly visible exposed parts of the first layer. After a second UV exposure, a second post exposure bake, development, rinsing and a hard bake follow. The master can then be used to manufacture a PDMS mold in a custom plexiglas mold: It is placed in the plexiglass mold and mixed PDMS is poured onto the master (Figure 10.3 (a)). After removing bubbles in a vacuum chamber and curing at 70° for 45 min, the new PDMS mold can be removed from the plexiglass mold. Four holes have to be punched that allow to run the inlet and outlet tubing through the polyurethane afterwards, as indicated in Figure 10.3 (d). After placing the knotted tubing, the PU cast can be mixed and poured into the mold. The vacuum chamber removes bubbles. It might be necessary to use the rubber piston of a syringe to remove air bubbles that stick in the features of the mold. The PU has to cure for 2 hours at a temperature of $150°C$. After a cool-down, the storage layer is ready for a surface treatment.

Figure 10.3: *Manufacturing the storage layer: (a) A PDMS mold is produced, (b) & (c) The mold is used to cast the storage layer from polyurethane, (d) Before casting, the tubing (with a knot to prevent slipping out) is inserted through holes in the mold (e) and cut after curing after curing the polyurethane*

10.1.4 Surface Treatment of the Storage Layer

When loading an untreated chip with protein, a silky surface forms on the sample droplets (Figure 10.4). We assume that this is caused by partial denaturation of the protein. The proteins tend to stick on the polyurethane such that the loading does not work properly: Channels become more hydrophilic and the individual sealing of the samples does not work. To prevent sticking and denaturation, the PU storage layer was treated with Cytop, which deposits a thin layer of Teflon onto the channels, making them hydrophobic.

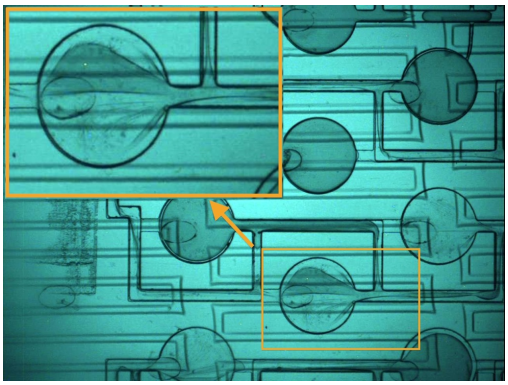

Figure 10.4: *Chip without surface treatment: Proteins (myoglobin in this image) denaturates, leaving a silky surface that causes malfunction of the storage layer*

List of Materials:

- Oven (150°C)
- Cytop 809M from AGC Chemicals Europe, Ltd.
- Tubing, Cole Parmer PEEK, 300 μm inner diameter

To perform the Cytop treatment, a few drops of the Cytop solution have to be dripped on top of the storage layer such that the solution creeps into all features. It is helpful to use a piece of tubing to spread the solution. The storage layer is baked at a temperature of 150 °C for 30 minutes and cooled down afterwards. The tubing hast to be cut as indicated in Figure 10.3 (e), the storage layer is ready for use.

10.1.5 Membrane and Teflon Foil Fabrication

The membrane was cut to proper size from a membrane sheet and pierced with a hole puncher. The Teflon foil was microperforated using a laser cutter at Harvard University.

10.2 Assembling the Phase Chip

To prevent contamination of the sample and to get a clear view under the microscope, the chip components need to be cleaned in a sonicator before the assembly. The cleaning solution contains:

- 300 ml destilled water
- ca. 500 μl Helmanix
- ca. 250 mg Zonyl FSN

All components have to be sonicated for at least 15 minutes and rinsed afterwards with destilled water.

Items that are needed for the assembly of the phase chip:

- Chip components
- FC-43 oil
- Tubing, Cole Parmer PEEK, 300 μm inner diameter
- Screwdriver
- Microscope
- 4 screws

To start the assembly of the chip, the bottom plate, the reservoir and the storage layer have to be dried by compressed air. The tubing is plugged into the reservoir layer in- and outlets and inserted through the bottom plate. The reservoir is placed on top such that the through holes of the reservoir and the bottom-plate align. The membrane is taken out of the water and dried with a wipe. When placing the membrane on top of the reservoir, it still has to be wet and turbid. 200 μl of FC-43 have to be dropped and spread on the membrane to protect it from drying out. The Teflon foil is placed on top of the membrane, followed by the storage layer. All four screws are inserted and tightened a little such that the Teflon foil is still loose enough to be shifted into position. It is important to double-check if the Teflon foil aligns with the holes before inserting the screws, since the foil can easily get pierced. The oil helps to shift the foil smoothly and precisely. Under a microscope, the foil is aligned with the storage layer such that every perforation matches one storage well (see Figure 10.6). Applying a little pressure with a finger on this “sandwich” helps tightening the screws without shifting any of the component out of position. The reservoir can be used as an indicator to find the right amount of contact pressure. As soon as the screws were tightened too much, the reservoir channels deform, yielding increased flow resistance, which is not favorable. Ideally the contact pressure should be as low as possible but still enough to prevent leaks. A very light deformation is unavoidable since the storage layer as well as the reservoir layer are not perfectly even (see Figure10.7). The whole process of the assembly was documented in Figure 10.5 (a)-(g).

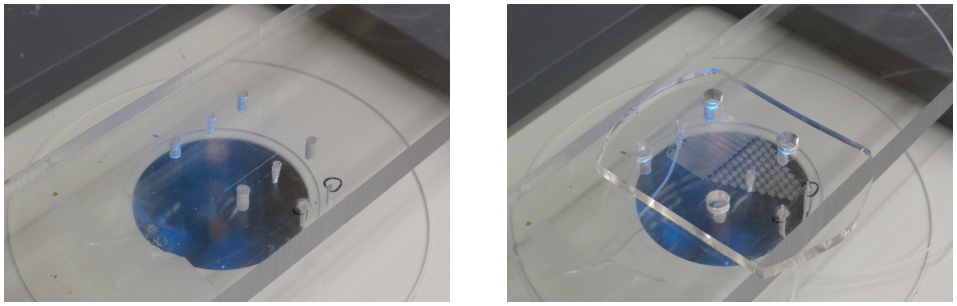

(a)

(b)

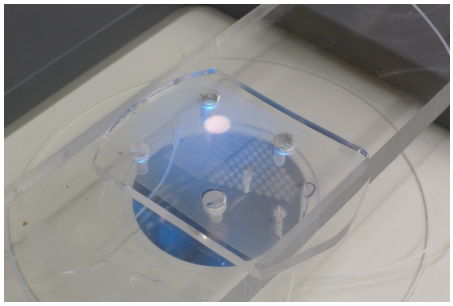

(c)

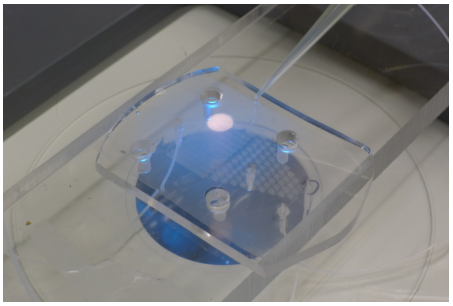

(d)

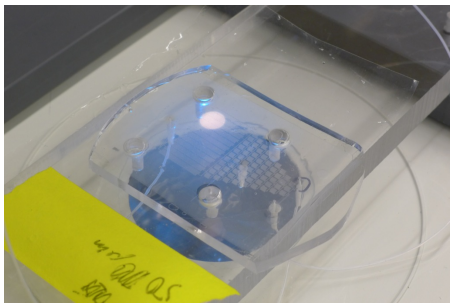

(e)

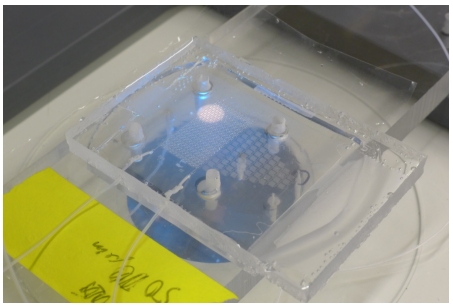

(f)

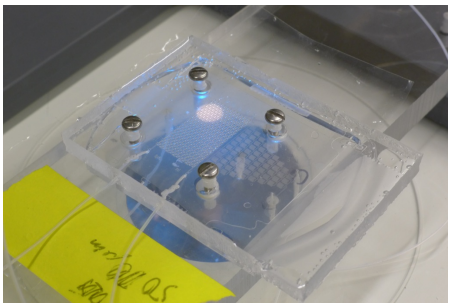

(g)

Figure 10.5: *Assembly of the phase chip: (a) Bottom piece, (b) Placing the reservoir, (c) Adding the membrane, (d) Depositing FC-43 onto membrane, (e) Placing the foil, (f) Placing the storage layer, (g) Tightening screws after the alignment*

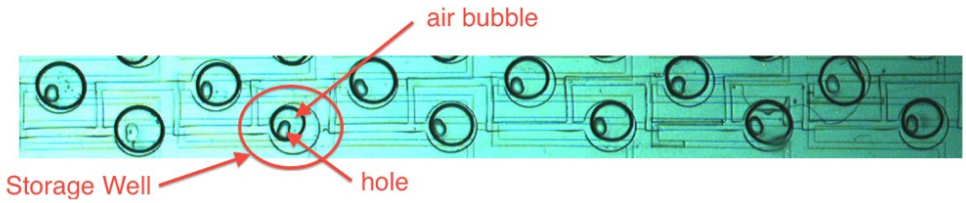

Figure 10.6: *Components of the chip aligned properly: Every perforation in the foil matches one storage well. Possibly air bubbles get trapped in the storage wells during the alignment.*

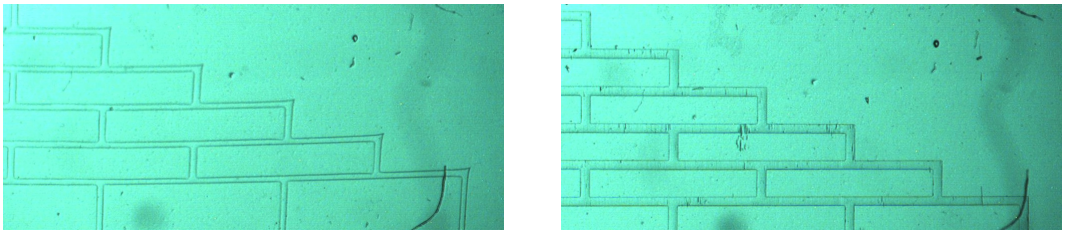

(a) (b)

Figure 10.7: *Reservoir as indicator for proper contact pressure provided by the screws in chip assembly: (a) Screws tightened too much, (b) Deformation has to be as low as possible without leaking*

10.3 Application of the Phase Chip

This section describes methods in the application of the phase chip.

10.3.1 Preparing the Chip for Loading

List of Materials

- 2 Syringe Pumps
- FC 43 oil
- 2 Syringes, $1ml$
- Tubing, Cole Parmer PEEK, 300 μm inner diameter
- Razorblade
- Screwdriver
- Sample solution

The storage layer and the reservoir layer are connected to syringe pumps filled with FC 43 and the reservoir solution, a small PMDS cube with a through-hole is used as a connector (plugged PDMS connector cube shown in Figure 10.10). The air bubbles that were trapped during the assemby have to be removed and the empty reservoir has to be filled: Both pumps are set to a flow-rate of 1000 μl/h. The flow carries most of the trapped air bubbles out of the chip. A small amount of the air dissolves in either the water, the oil or the material of the chip. As soon as only a few bubbles remain or their size does not change anymore, the outlets of the chip are blocked using plugged PDMS connectors. This helps to raise the pressure and the air bubbles dissolve more quickly. The pumps are turned off as soon as there is no air neither in the chip nor in the tubing. All outlets have to be opened to let the pressure settle. The chip is ready for loading.

10.3.2 Loading a Sample

Every storage well can hold 288 droplets of a volume of ca. 20 nl. At a total number of 288 storage wells, a total volume of less than 6 μl is sufficient to fill all 288 storage wells. The following section explains the loading procedure in practice.

To load the chip, the sample has to be brought into the inlet tubing of the chip first:

20 cm of tubing have to be attached to a 1 ml syringe, that was previously filled with FC-43. By gently pushing the piston, the tubing is filled with oil completely. The open end of the tubing is dipped into the sample. By pulling the piston gently outwards, a small amount of the sample is drawn into the tubing without trapping an air bubble between the oil phase and the sample. A minimum of 8.5 cm of the tubing has to be filled to load all storage wells. A higher amount is uncritical: As soon as all storage wells were filled, any excessive sample volume is flushed out of the chip. The tubing is then taken out of the sample and the inlet tubing of the storage layer is disconnected from the syringe pump and connected to the sample tubing. Air must not be trapped between sample and oil (Figure 10.11): It is helpful to squeeze the PDMS connector on the inlet tubing a little until a small amount of oil exits its open end and forms a little drop. Tapping on the piston of the syringe helps to bring the sample meniscus to the very end of the sample tubing: It is now plugged into the connector, through the little oil drop. The sample tubing is cut halfway between the syringe and the sample and connected to the syringe pump by a second PDMS connector. The procedure is illustrated in Figure 10.9.

Figure 10.8: *Sample in storage layer inlet tubing without trapped air: There must not be air bubbles between both liquid phases for proper loading*

The loading can now be started:

The syringe pump is used to drive the loading. Depending on the nature of the sample, flow-rates between 5μl/h and 45μl/h have proven to be optimal. With increasing viscosity, smaller flow-rates are more favorable. It is easy to find the optimal flow-rate during the loading process: The aqoueous phase must never pass through the capillary valve as explained in Section 4.1. If the valve breaks through, the flow-rate has to be reduced. A value of 5μl/h has worked with any sample that was used. The only reason to run at higher flow-rates is to reduce the loading time. There is time to find a good flow-rate until the whole sample passed through the chip and the oil phase enters. After that point, an excessive flow-rate would flush the storage wells. Ideally, a loaded chip should look as shown in Figure 4.4. The only hydrophilic region inside the storage well is the membrane. Thus the droplets automatically connect to the membrane during the loading procedure which is the requirement for osmosis with the reservoir. The pump has to run until there is only oil left in the outlet tubing and any residual sample has been flushed out.

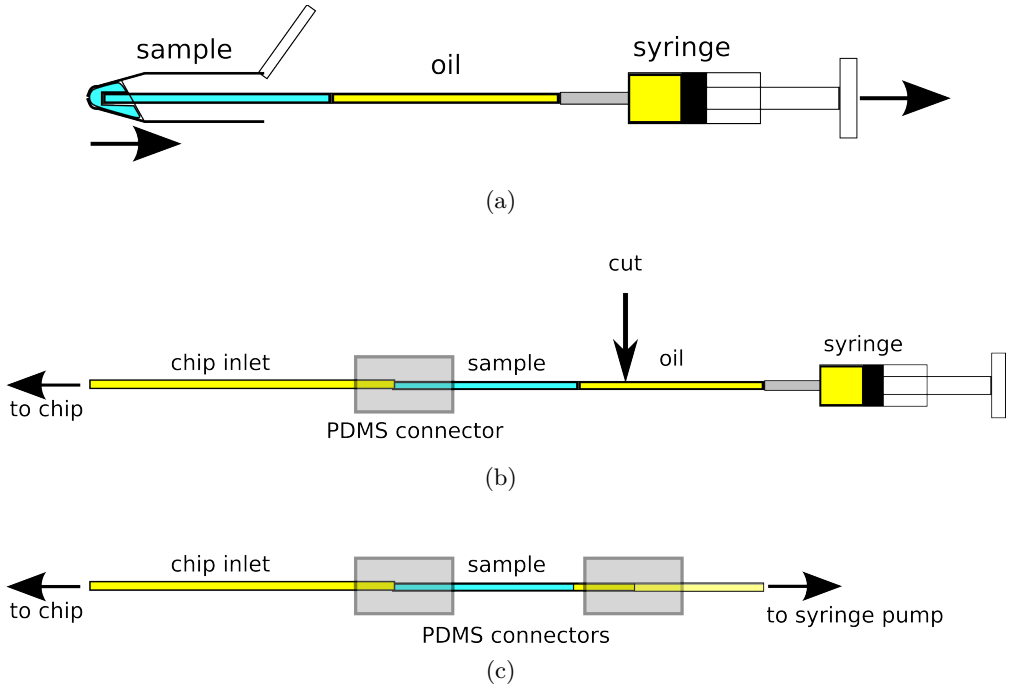

Figure 10.9: *Preparing a sample for loading: (a) Drawing the sample into a piece of tubing that was previously filled with FC 43 using a syringe, (b) Connecting the tubing to the storage layer inlet by a PDMS connector and cutting the sample tubing halfway between the sample and the syringe, (c) Connecting sample tubing to syringe pump by a second PDMS connector*

10.3.3 Transferring the Chip Between Setups

It is necessary to transfer the chip between different setups, for example between different microscopes or from a pressure driven to a flow driven setup. Before transferring, the storage layer outlet tubing has to be plugged very carefully using a plug as shown in Figure 10.10: When plugging it into the PDMS connector attached to the outlet, the plug acts act as a piston, causing flux that may flush out the loaded samples. The inlet tubing of the storage layer is then cut to avoid fluxes. The reservoir layer is not sensitive to pressure fluctuations and can therefore just be unplugged from the pumps without any further measures. The chip is now stable for a transfer. After the transfer, the connecting of the storage layer has also to be done very carefully as well to prevent the storage wells from flushing.

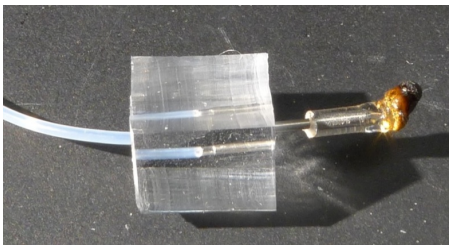

Figure 10.10: *PDMS connector and plug for blocking outlets*

10.4 Extracting Crystals from the Phase Chip

To analyze crystals in a syncrotron beam, crystals have to be isolated from the phase chip. In case that a constant reservoir was used, crystals in the chip were all grown under the same conditions. The procedure to isolate the crystals in this case is as follows: The chip has to be opened and flipped such that the storage layer is located at the bottom. All components are removed except the storage layer. The storage layer is then placed under a microscope and a puddle of cryo protectant is leveled on top of the features. Nylon loops, that are also used for isolating crystals grown by conventional methods, were convenient for extracting crystals from the phase chip. The course of action is shown in Figure 10.12. Crystals have to be frozen immediately after looping using liquid nitrogen. This conserves them until they are exposed to the syncrotron beam.

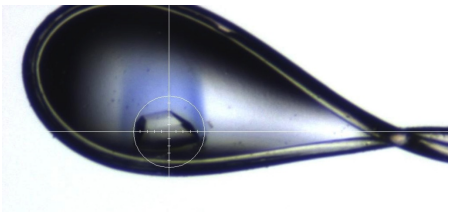

Figure 10.11: *Frozen glucose ismoerase crystal in a 300μm loop, surrounded by cryo protectant*

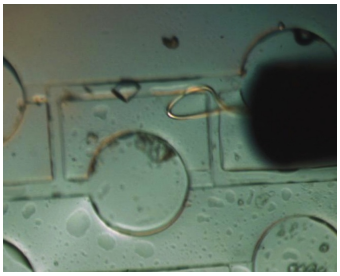

(a)

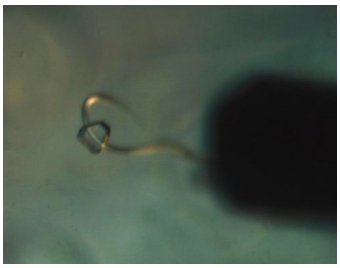

(b)

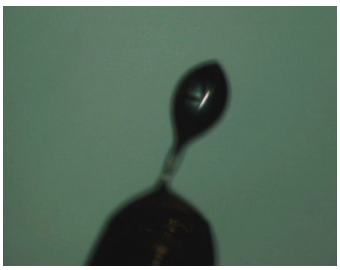

(c)

(d)

Figure 10.12: *Looping crystals from the phase chip: (a) Gently lift a crystal, (b) Direct the crystal to the surface of the puddle of cryo protectant, (c) Catch the crystal, (d) Drain excessive solution using a dental paper wick*

10.5 Growing D1D2 Crystals by Conventional Methods

Together with Michael Heymann and in collaboration with Prof. Dr. Daniel Pomeranz Krummel and Kelsey Anthony from the Biochemistry Department at Brandeis University, the influence on different polymer concentrations versus the influence of pH on the crystallization of the D1D2 heterodimer was screened by vapor diffusion (sitting drop method). The reservoir solutions that we used contained the following ingredients:

- 0.2 M ammonium acetate
- 15 w% glycerol
- 0.1 M sodium citrate, pH levels of 5, 5.2, 5.4, 5.6, 5.8, 6.
- PEG 4000, concentrations of 15%, 18%, 21%, 25%, 27%, 30%, 33%, 36%

This yields a total of 40 different reservoir solutions of varying polymer concentration versus varying pH. We set up trays using conventional pipetting (Figure 10.13 (a)) as well as another robot tray (Figure 10.13 (b)) using a pipetting robot. The reservoirs of the trays were filled with the above solutions, the wells were filled with a 1:1 mixture of the respective reservoir solution and the protein solution (7.5 g/ml of D1D2, 20 mM Hepes @ pH 7.0, 200 mM NaCal). The volumes of the protein solutions were $1\mu l$ in both trays. They were placed in a cabinet at room temperature.

Results from manual tray: Pictures of wells that contained crystals were taken after one week: D1D2 crystallizes in vapor diffusion within one week at a minimum polymer concentration of 25 w% PEG 4000. Most of the crystals look like a double crystal of two single crystals merged at their

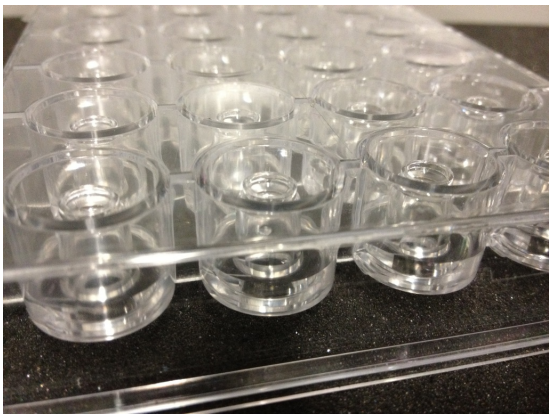

(a)

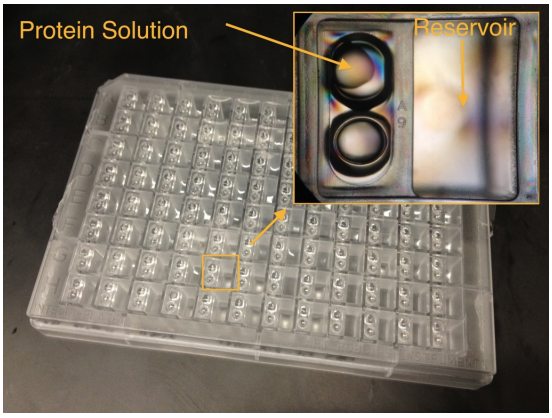

(b)

Figure 10.13: *Trays for sitting drop method: (a) shows a robot tray and (b) a tray for manual pipetting.*

tips (Figure 10.14 (c)). Single crystals were obtained from a polymer concentration of more than 30 w% PEG 4000. All images of crystals in this section were taken at the same scale for comparable sizes.

At a polymer concentration of 25 w% PEG 4000, only double crystals were obtained from pH 5-5.6. With increasing pH, the number of crystals decreases and their size increases. At pH 5.6, a star-like multiple crystal appeared. (Figure 10.14)

At 27 w% PEG 4000, only pH 5.6 and 5.8 yielded many tiny double crystals (Figure 10.15).

At 30 w% PEG 4000, crystals were only obtained from pH 5.8. They seem to be single crystals (Figure 10.16).

33 w% PEG 4000 yielded medium crystals only at pH 5.6, that were single (Figure 10.17).

A polymer concentration of 33 and 36 w% yielded medium and small crystals only at pH 5.6, that were also single (Figure 10.17).

The observations are summarized in Table 10.1.

Table 10.1: *Summary of the conditions in vapor diffusion that yielded D1D2 crystals: The size refers to the relative size compared to all crystals from the tray. "Double", "single" and "star" refer to the text.*

	pH = 5.0	pH = 5.2	pH = 5.4	pH = 5.6	pH = 5.8	pH = 6.0
15 w% PEG 4000						
18 w% PEG 4000						
21 w% PEG 4000						
25 w% PEG 4000	medium, double	medium, double		medium, double	big, star	
27 w% PEG 4000					small, double	small, double
30 w% PEG 4000				medium, single		
33 w% PEG 4000				medium, single		
36 w% PEG 4000				small, single		

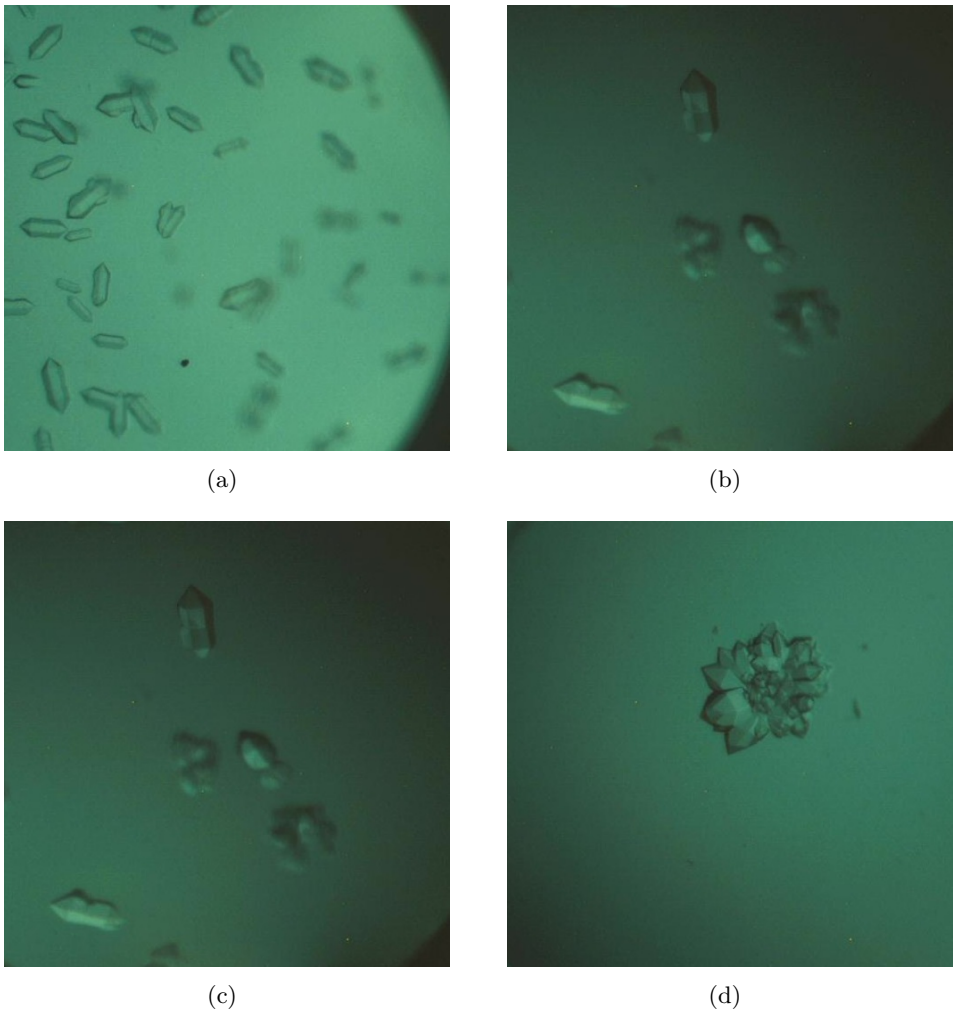

(a) (b)

(c) (d)

Figure 10.14: *D1D2 crystals from vapor diffusion at 25 w% PEG 4000: (a) pH 5.0, (b) pH 5.2, (c) pH 5.4, (d) pH 5.6*

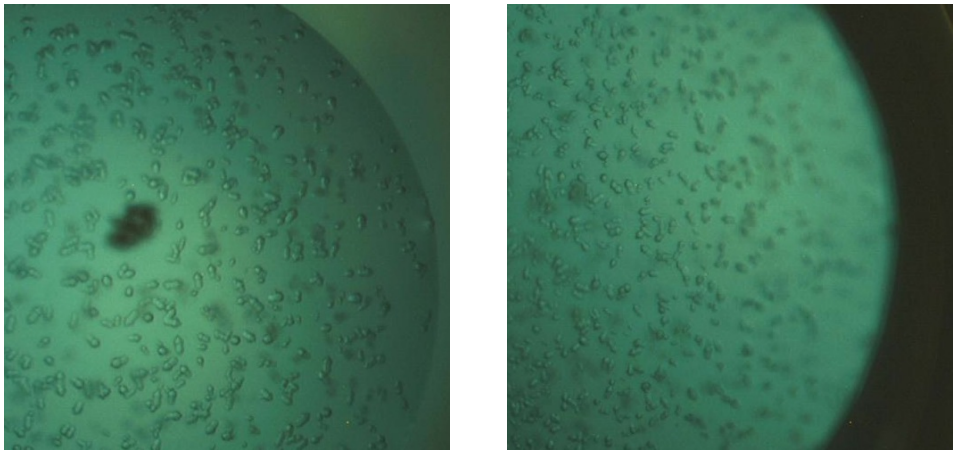

(a) (b)

Figure 10.15: *D1D2 crystals from vapor diffusion at 27 w% PEG 4000: (a) pH 5.6, (b) pH 5.8*

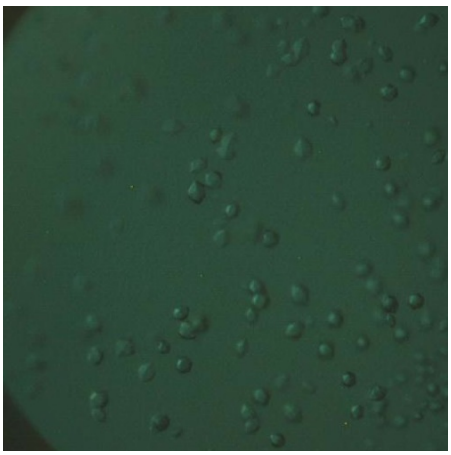

Figure 10.16: *D1D2 crystals from vapor diffusion at 30 w% PEG 4000: pH 5.6*

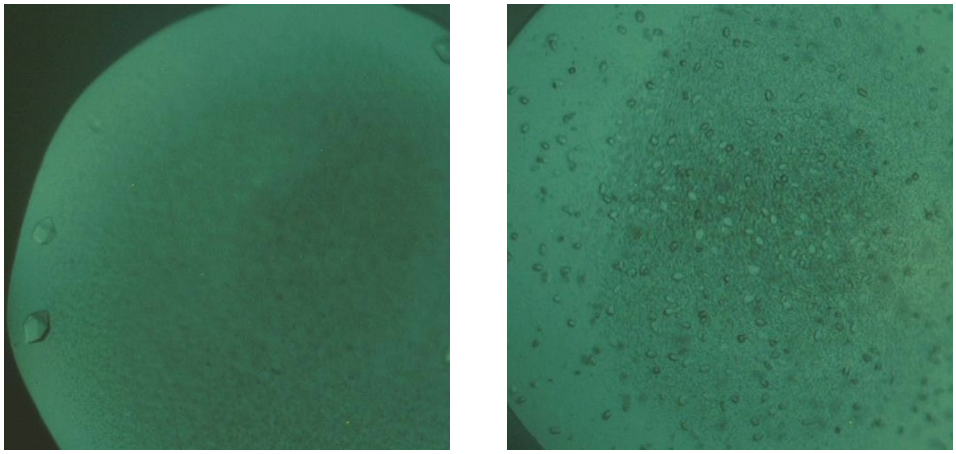

(a) (b)

Figure 10.17: *D1D2 crystals from vapor diffusion at pH 5.6: (a) 33 w% PEG 4000 , (b) 36 w% PEG 4000*

10.6 A New Method for the Fabrication of the Storage Layer

The Cytop surface treatment of the storage layer proved to wear out after a few applications. It is therefore suggested to fabricate the storage layer directly from a block of Teflon by hot embossing. The use of a Teflon storage layer would make secondary surface treatments unnecessary. To hot emboss Fluorinated Ethylene Propylene (FEP), a master with enough tensile strength and cast from a material with a higher melting temperature then the glass transition temperature of FEP at 204 $°C$ is needed. For this means, a master was build from copper by electroplating onto a PDMS replica from a SU8 master fabricated using standard soft-lithography (Figure 10.18). To prime the non-conducting PDMS surface, a thin silver layer was first deposited onto the PDMS cast using the Tollens' reaction.

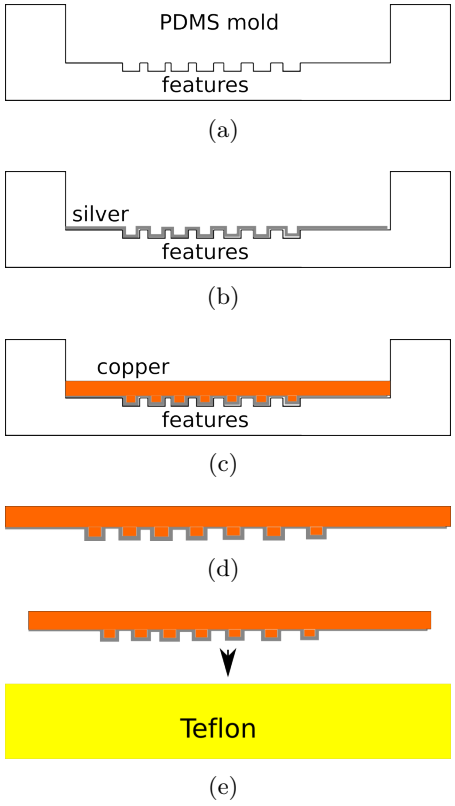

Figure 10.18: *Fabricating a stamp for the production of the storage layer by hot embossing Teflon: (a) PDMS mold, (b) Deposit silver onto features to provide conductivity, (c) Deposit copper onto silver using electroplating, (d) Lift off the stamp, (e) Emboss Teflon*

The feasibility of this process was proved with the following protocol. Solutions used:

- 0.6 M silvernitrate in water
- 2 M sodium hydroxide in water
- 28% ammonium hydroxide
- 0.05 M glucose in water

A PDMS Mold was fabricated and bonded to a cover glass slide to prevent buckling. A few drops of the sodium hydroxide solution were mixed with $2mL$ of the silvernitrate solution. A brown precipitation appeared. Carefully adding drops of the ammonium hydroxide solution yielded a clear Tollens' solution. After a plasma treatment of the mold, $1mL$ of the glucose solution was poured into it and the Tollens' solution was added. Half an hour later, the solution was rinsed out with water, leaving a thin silver layer inside the mold. The mold was then placed in a copper bath, containing the following ingredients:

- 60 g $CuSO_4$
- 30 g Ethanol
- 25 g H_2SO_4
- 500 ml Water

An unisolated braid was placed on top of the silver and connected to the negative pole of a power supply. A copper plate was placed 1 cm above the silver surface and connected to the positive pole. The power supply was set to 1V. After 24 hours, the mold was disconnected from the power supply, the copper stamp was removed from the mold and placed on a 5 mm thick teflon block between two layers of kapton. This sandwich was then pressed by two 500 g weights and incubated at a temperature of $270°C$ for 15 minutes. After cooling down, the copper stamp was removed and embossed features appeared on the Teflon. The whole process is documented in Figure 10.19.

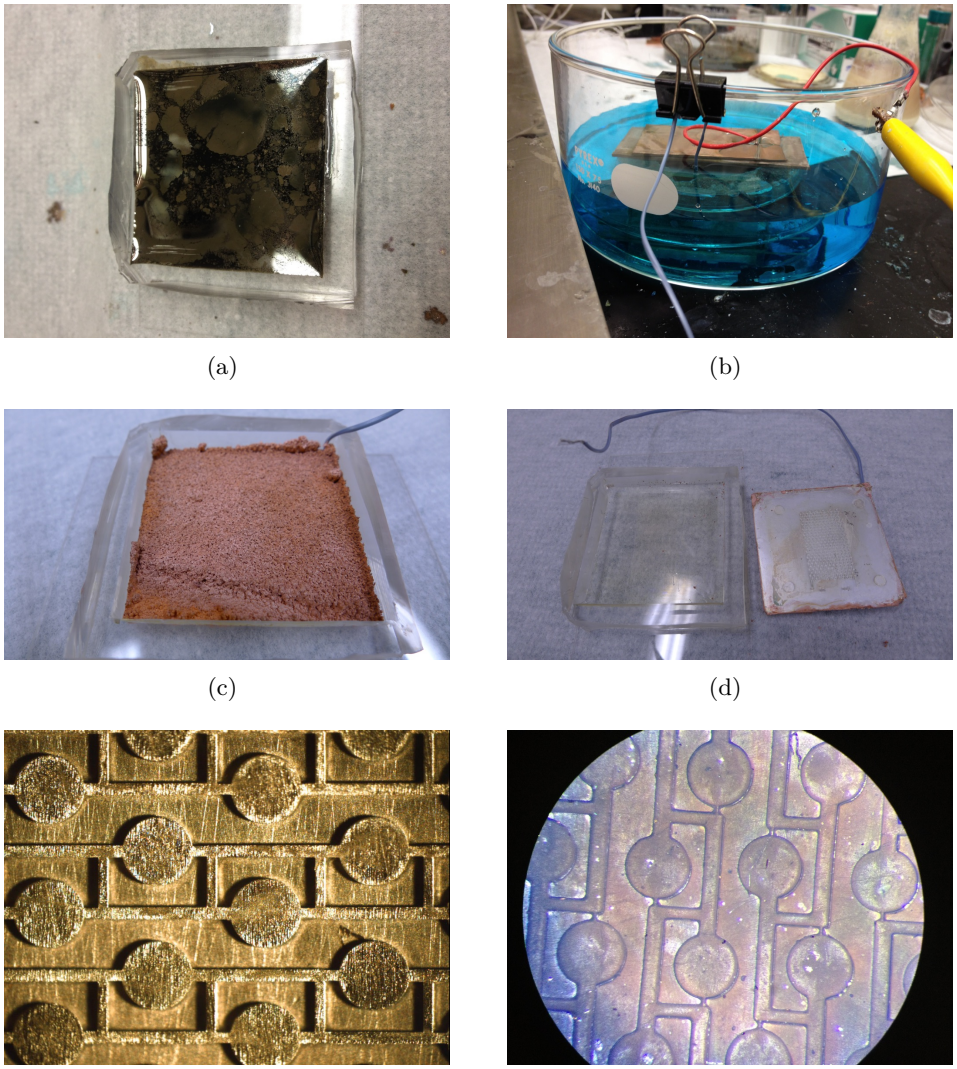

Figure 10.19: *A copper stamp for hot embossing made from a PDMS mold: (a) Depositing silver onto features in PDMS mold using Tollens' reaction, (b) Electroplating copper onto silver layer, (c) Copper stamp in mold after electroplating, (d) Copper stamp after lift-off, (e) Close-up of the features in the copper stamp, (f) Features embossed in Teflon*

10.7 Description of Matlab Algorithm for Measuring Growth Rates of the Droplets in the Storage Layer

A code was written in Matlab to determine transport fluxes of water through the membrane by measuring growth rates of the droplets in the storage layer from time lapse images. A brief description of the function can be found in Figure 10.20. An uncommented raw version of the code that was written is attached in Section 11.1 in the listings 1, 2 and 3.

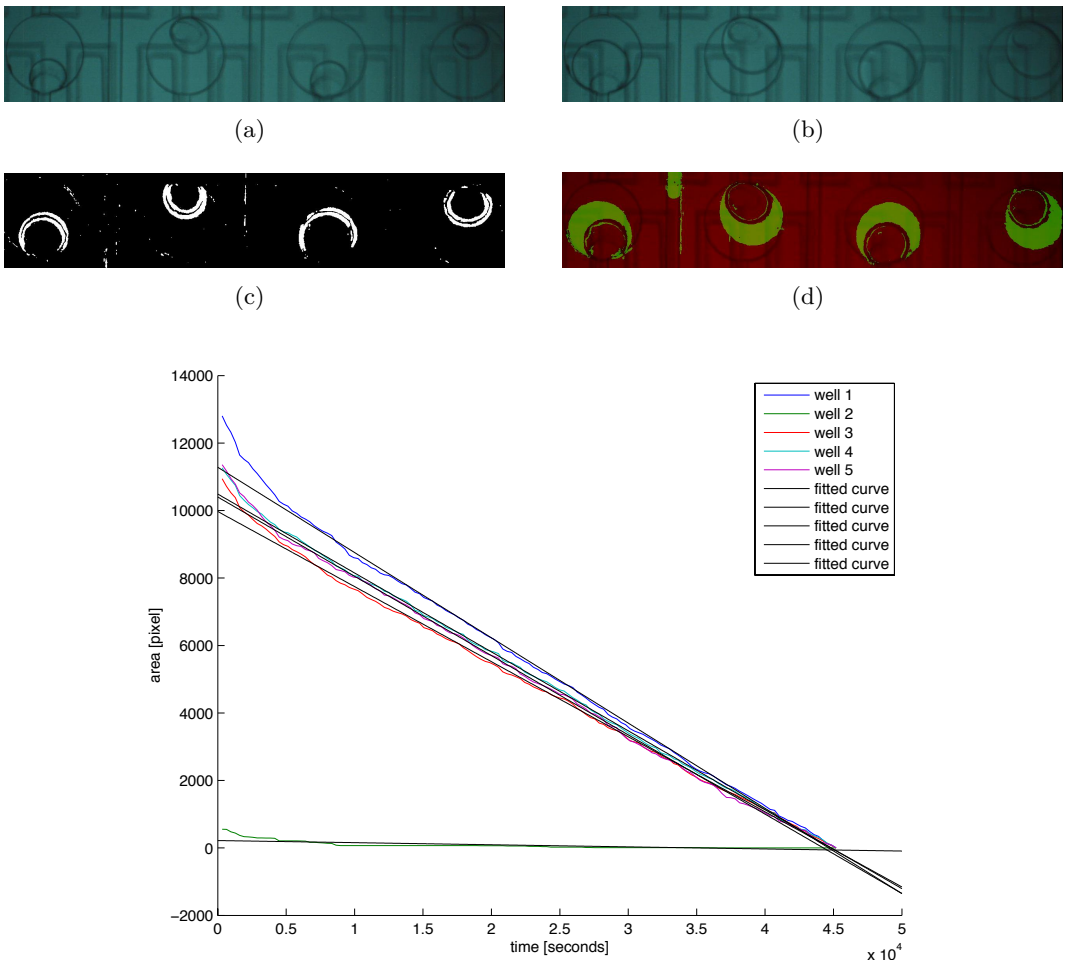

Figure 10.20: *Visualization of the function of the Matlab code to measure growth rates of droplets in storage wells from time lapse images. (a) First raw image in time lapse data series: Circumference of the droplet is visible, (b) Last raw image in time lapse data series: Droplets grew. (c) Recognition of moving edges by evaluation of the whole time lapse image series; Measuring area of droplets per time: (d) Green area was swept out by moving edge. Moving edge is continously subtracted from green area while resulting green area is calculated. (e) Plot of the resulting areas over time and linear fits: Slopes are always negative in this algorithm, also for growing droplets. The sign has to be determined manually. Well 2 is an artifact of a moving liquid in one of the channels.*

11 Appendix

11.1 Matlab Source Code

```
%% Main programm for determining the growth rate of droplets in pixels per second from time lapse images
%% Specify in code: Base directory with time lapse images, im2bwparameter (bewtween 0 and 1) and skip1= (between 1 and the number of images - 1)
%% Specify in dialog: Duration of experiment
%% Will output processed data and a readme file as explanation

im2bwparameter = 0.73;

skip1 = 30 ; %number of frames to skip for subtraction to calculate edges:


%% Start dialog
base = '/Users/markusludwig/Desktop/Labor/data/' ; %define base directory with images to be analysed
listing = dir(base);
images = [];
rgb = 3; % choose rgb channel 3

prompt = {'Enter period of obeservation in seconds'};
dlg_title = 'Calculating timestep';
num_lines = 1;
time = inputdlg(prompt,dlg_title,num_lines); %get period of observation
timestep = str2double(time{1}) /(size(images,3));%calculate period between two images

prompt = {'Any comments to add to readme.txt?'};
dlg_title = 'Any comments to add to readme.txt?';
num_lines = 1;
comment = inputdlg(prompt,dlg_title,num_lines); %get comments to add to readme file later


%% Parameters that control edge recognition:

%% Read images and import
for i = 3:length(listing)
    name = listing(i).name;
    % verify that file to process is a .jpg:
    [junk1, junk2, ext] = fileparts(name);
    if strcmp(ext, '.jpg')~=0
        disp(name);
        %create image array if it doesnt exist already
        if isempty(images)
            tmpimg = imread([base name]);
            tsize = size(tmpimg);
            images = zeros(tsize(1), tsize(2), length(listing)-3);
        end
        %write images into 3 dim array
        tmpimg = imread([base name]);
        images(:,:,i-3) = tmpimg(:,:,rgb);
    end
end
images(:,:,:) = images(:,:,:)/255; % 8 bit for each color channel = 0, .... 255 -> 0, .... ,1


%% Recognition of droplet edges and calculation of a region of interest

images_1 = images; % new array for manipulation of images
total_lost_images = 0;
[images_1, lostimages] = findedges(images,im2bwparameter,skip1);
total_lost_images = total_lost_images+lostimages;

%create roi = region of interest
roi = zeros(size(images_1,1),size(images_1,2));

for i = 1:size(images_1,3)-1
```

```
    if sum(sum(images_1(:,:,i)-
        images_1(:,:,i+1))) > 1000
        images(:,:,i+1) = 0;
    end
end


%Include all edges from all images
    into one image to generate region
    of interest
for i = 1:(size(images_1,3))
    roi = roi + images_1(:,:,i);
end
roi = im2bw(roi, 0.1); % normalize
    to 1 or 0 values
roi = bwareaopen(roi,500); % delete
    spots with less than 500 pixels
roi = im2bw(roi,0.5);


rmdir('OUTPUT', 's');
mkdir('OUTPUT');
roifilled = zeros(size(images_1,1),
    size(images_1,2));
se3 = strel('disk',10);
roifilled = imdilate(roi, se3);
mkdir('OUTPUT/ROI/');
filename = ['OUTPUT/ROI/' 'ROI' ];
imwrite (roi, filename, 'jpg');
filename = ['OUTPUT/ROI/' 'ROIFilled
    ' ];
imwrite (roifilled, filename, 'jpg'
    );
display ('roi done');


%%%write "dropletfront multiplied by
    roifilled" to file to check

imout = zeros(size(images_1,1),size(
    images_1,2));

for i = 1:size(images_1,3)
    mkdir('OUTPUT/detected edges/');
    filename = ['OUTPUT/detected
        edges/' listing( i + 2 ).name
        ];
    imout = im2bw(images_1(:,:,i)+
        imout);
    %imout = im2bw(roi .* (images_1
        (:,:,i)+imout ),0.1);
    imwrite (imout, filename, 'jpg'
        );
end


display ('extracting edge done');


%% Calculates areas of droplets

cc = bwconncomp(roifilled, 4);
numberofwells = cc.NumObjects; %
    Number of droplets

area = zeros (size(images_1,3),
    numberofwells,2);
display ([ num2str( numberofwells) '
    wells detected' ]);
well_id = zeros(size(images_1,1),
    size(images_1,2),numberofwells);

timestep = str2double(time{1}) /(
    size(images,3)-1); % calculates
    the time per image


for i = 1:numberofwells
    well_x = false(size(roi));
        %
    well_x(cc.PixelIdxList{i}) =
        true;
    temp = zeros(size(images_1,1),
        size(images_1,2));
    well_id(:,:,i) = well_x;
    temp = roi.*well_x;
    mkdir('OUTPUT/
        Well_identification/');
    filename = ['OUTPUT/
        Well_identification/' 'well
        number' num2str(i) ];
    imwrite (temp, filename, 'jpg')
        ;
    for j = 1:size(images_1,3)
        temp = im2bw(temp - images_1
            (:,:,j),0.1);
        area(j,i,1)=sum(sum(temp));
            %count number of pixels
            that have the value 1
        area(j,i,2)= timestep*j ;
    end
    display (['well number ' num2str
        ( i) ' done' ]);

end

%% Plot

h = figure; %forces open new figure
```

```
%subplot (2,2,[1 2]);
hold on;

plot(area(:,:,2),area (:,:,1));
csvwrite('OUTPUT/Area',area);

names = cell(numberofwells, 1);

for i = 1:numberofwells
    names{i} = ['well ' num2str(i)];
end
legend(names, 1);

fit_parameters = zeros(3,
    numberofwells);

for i = 1:numberofwells

    xdata = area(:,i,2); %time
    %xdata = transpose(xdata);
    ydata = area(:,i,1); %area


    xdataderivative = diff(xdata);
    ydataderivative = diff(ydata);

    quart = zeros(1,2);
    quart(:) = quantile(
        ydataderivative,[.2 .8]);


    l=0;

    for k = 1: size(ydataderivative)
        if abs(ydataderivative(k)) >
             abs(quart(1))
            ydata(k-l) =[];
            xdata(k-l) =[];
            l=l+1;
        end
        if abs(ydataderivative(k))
            <= abs(quart(2))
            ydata(k-l) =[];
            xdata(k-l) =[];
            l=l+1;
        end
    end

    f = fittype('a*x+c');
    %lower bisquare weight in a
        robust fit:
    %fit1 = fit(xdata,ydata,f,'
        StartPoint',[1 1],'Robust','
        on');
    fit1 = fit(xdata,ydata,f,'
        StartPoint',[1 1]);
    ci = confint(fit1);
    confidencebounds = ci(:,1);


    plot(fit1,'black');

    fit_parameters(1,i) = i;
    fit_parameters(2,i) = fit1.a; %
        Print slope
    fit_parameters(2,i) =
        fit_parameters(2,i) ;
    fit_parameters(3,i) = abs(
        fit_parameters(2,i)-
        confidencebounds(1,1)); %
        print standard deviation

end

xlabel('time [seconds]');
ylabel('area [pixel]');
hold off;
csvwrite('OUTPUT/slope',
    fit_parameters); %print fitslope
    & error for each well to csv file
print(h,'-dpsc','OUTPUT/Graph') %
    print to postscript file

%subplot (2,2,3); imshow (roifilled)
    ;
%subplot(2,2,4);

pic = zeros(size(images,1),size(
    images,2));
H1 = gca;
areaim = roi;

for i = 1:size( images_1, 3 )
    set( gca, 'Zlim', [-20, 20] );
    collage = zeros (size(images_1
        ,1),size(images_1,2),3);
    collage (:,:,1) = images(:,:,i+
        skip1)*1;
    areaim = areaim - images_1 (:,:,
        i);
    areaim = im2bw (areaim, 0.1);
    collage (:,:,2) = areaim.*0.5;
    mkdir('OUTPUT/movie');
    filename = ['OUTPUT/movie/' '
        frame' num2str(i) ];
    imwrite (collage, filename, '
        jpg');
end
```

```
223
225
%%print text file for explanation of
    OUTPUT files
227 fileID = fopen('OUTPUT/readme.txt','
    w');
fprintf(fileID,'**** IM2BW threshold
    @ ');
229 fprintf(fileID,num2str(
    im2bwparameter));
fprintf(fileID,'**** Time @ ');
231 fprintf(fileID,num2str(skip1));
fprintf(fileID,'**** skip @ ');
233 fprintf(fileID,char(time));
fprintf(fileID,' sec');
235 fprintf(fileID,'\r\n\r\n');
fprintf(fileID,'AREA.csv**** first n
    /2 of n columns represent the
    area, the second n/2 columns
    represent timesteps of raw data
    for each well,\r\nUNITS are in
    pixels or in seconds respectively
    ');
237 fprintf(fileID,'\r\n\r\nSLOPE.csv
    **** identifies the number of the
     specific well as first value in
    each column, the second row
    represents the slope and the
    third row the error, \r\nUNITS
    are in pixels per second');
fprintf(fileID,'\r\n\r\n');
239 fprintf(fileID, char(comment));
fclose(fileID);
```

Listing 1: *Main Program*

```
%%Recognizes the edge of the
    droplets by subtraction of two
    images at a time distance "skip"
2
function [output, lostimages]=
    findedges(images,im2bwparameter,
    skip) % function outputargument =
     name(input)
4
for i = 1:size( images, 3)-skip
6     images(:,:,i) = abs(images(:,:,i
          )- images(:,:,i+skip)); %
          subtracts images at the
          distance "skip", result will
          be the edges of drop, if "
          skip" is bigger then
          regognition works better but
          also edges are less precise
8     images(:,:,i) = normalization(
          images(:,:,i)); %normalizes
          image
      images(:,:,i) = medfilt2(images
          (:,:,i)); %reduce noise
      images(:,:,i) = im2bw(1-images
          (:,:,i),im2bwparameter); %
          edges will appear white at
          black background
10    images(:,:,i) = (1-bwareaopen(
          images(:,:,i),60)); % erases
          all areas smaller than 60 pix
end
12
 display ('edges found');
14
 output = images(:,:,(1:size(images
     ,3)-skip));
16 lostimages = skip; % number by
     which the number of output
     images compared to number of
     input images is reduced from
     this operation

18 end
```

Listing 2: *Edge Recognition*

```
%%Normalizes pixel intensities to a
    range of [0,1]
2 %%
function xnorm = normalization(x) %
    function outputargument = name(
    input)
4
xmin = min(min(x));
6 xmax = max(max(x));

8 if xmin == xmax
    % Constant matrix -> warn and
        return a NaN matrix
10  warning('normalization:
        constantMatrix', 'Cannot
        normalize a constant matrix
        to the range [0, 1].');
    xnorm = nan(size(x));
12
else
14  b(:,:) = xmin;
    xnorm = (x-b)./(xmax-xmin);
16 end
```

Listing 3: *Normalization of Images*

List of Figures

List of Tables

12 References

[AO54] Asakura, S. ; Oosawa, F.: Interaction between two bodies immersed in a solution of macromolecules. In: *J Chem Phys* (1954)

[Ash04] Asherie, N.: Protein crystallization and phase diagrams. In: *Methods* (2004)

[Ber03] Bergfors, T.: Seeds to crystals. In: *Journal of Structural Biology* 142 (2003), S. 66–76

[BSJ+09] Boukellal, H. ; Selimovic, S. ; Jia, Y. ; Cristobal, G. ; Fraden, S.: Simple, robust storage of drops and fluids in a microfluidic device. In: *Lab on a Chip* (2009)

[Dem05] Demtröder, W.: *Experimentalphysik 1, Mechanik und Wärme*. Springer Berlin Heidelberg New York, 2005

[elv] `http://ucxray.berkeley.edu/~jamesh/elves/manual/index.html`

[GR03] Garcia-Ruiz, J. M.: Nucleation of protein crystals. In: *Journal of Structural Biology* (2003)

[KZ01] Kulkarni, A. ; Zukoski, C.: Depletion interactions and protein crystallization. In: *Journal of Crystal Growth* (2001)

[Leu01] Leunissen, M.: An essay on several aspects of protein crystallization research. In: *University of Cambridge, Department of solid state chemistry* (2001)

[loa] `http://www.technologynetworks.com/loac/`

[Mes06] Meschede, D.: *Gerthsen Physik*. Bd. 23. Springer, 2006

[MHA00] Mathews, C. K. ; Holde, K. E. ; Ahern, K. G.: *Biochemistry*. Benjamin/Cummings Publishing Co., Inc., 2000

[mic] `http://microchem.com/pdf/SU-82000DataSheet2025thru2075Ver4.pdf`

[mit] `http://www.mitegen.com/products/jen_screens/Background_Information.pdf`

[msd] `http://msdssearch.dow.com/PublishedLiteratureDOWCOM/dh_0889/0901b8038088978e.pdf?filepath=polyglycols/pdfs/noreg/118-01816.pdf&fromPage=GetDoc`

[nan] `http://nano.cancer.gov/action/news/featurestories/monthly_feature_2005_aug.asp`

[nyu] `http://physics.nyu.edu/grierlab/methods/node11.html`

[phy] `http://phycomp.technion.ac.il/~talimu/boltzman.html`

[RHSN93] Rosenberger, F. ; Howard, S.B. ; Sowers, J.W. ; Nyce, T.A.: Temperature dependence of proteinsolubility — determination and application to crystallization in X-ray capillaries. In: *Journal of Crystal Growth* (1993)

[Sel10] Selimovic, S.: *Microfluidics for Protein Crystallization and Mapping Phase Diagrams of Aqueous Solutions*, Brandeis University, Diss., 2010

[SGF12] Selimovic, S. ; Gobeaux, F. ; Fraden, S.: Mapping and manipulating temperature–concentration phase diagrams using microfluidics. In: *Lab on a Chip* (2012)

[SJF09] Selimovic, S. ; Jia, Y. ; Fraden, S.: Measuring the Nucleation Rate of Lysozyme using Microfluidics. In: *Crystal Growth & Design* (2009)

[Skj06] Skjæveland, S. M.: Derivation of the Laplace equation. (2006)

[TMS05] T. M. Squires, S. R. Q.: Microfluidics: Fluid physics at the nanoliter scale. In: *REVIEWS OF MODERN PHYSICS* (2005)

[VBTB02] Vivarès, D. ; Belloni, L. ; Tardieu, A. ; Bonneté, F.: Catching the PEG-induced attractive interaction between proteins. In: *THE EUROPEAN PHYSICAL JOURNAL* (2002)

13 Acknowledgments

First of all I would like to express my special gratitude to Prof. Dr. Seth Fraden for the chance to visit and to be a part of his lab. I thank him for the unlimited access to his research, for his patience and many deep and inspiring conversations, for taking me to several talks at Harvard University and for his generous hospitality.

I thank Prof. Dr. Georg Maret for his support and taking the time for establishing the contact with Seth Fraden, encouraging me in my intent for this stay abroad and assisting me in formal matters.

I would like to thank Michael Heymann for offering me unlimited possibilities in taking part in his research, for countless inspiring discussions, for his dedicated constructive feedback in the writing of this thesis. I thank Michael and his wife Aline Blunk for their hospitality.

To Prof. Dr. Daniel Pomeranz Krummel, I am grateful for guiding me in the making of buffer solutions, for inspiring conversations, for offering the option to work in his lab and the cold room. I thank Kelsey Anthony for teaching me how to set up sitting drop trays and to harvest their crystals. I am grateful for having had the chance to be part in the investigation of the D1D2 heterodimer.

To the rest of the Fraden Group, thank you for the cooperative atmosphere and for compensating leisure-times. Special thanks to Sathish Akella for his assistance in different matters, especially with the scanning stage. I thank him, Camille Girabawe and Bernard Hishamunda for their hospitality.

Roland Maher and David Elwell offered me an excellent support in formal matters of my stay and helped to provide financial support from the Physics Department at Brandeis. I would like to express my special gratitude to them.

I thank Greg Widberg for letting me take part in his machine shop course and for offering helpful advises during the manufacturing of chip components.

I would like to express my special gratitude the the DAAD for offering me financial support from a PROMOS stipend.

My warm and heartfelt gratitude goes to my parents Brigitte and Christoph Ludwig for the support they provided throughout my entire life. They have been a constant source of love, concern and strength.

To Magdalena Körber, I am grateful for her support in the correction of this thesis, for encouraging me constantly and helping me not to loose sight of things besides research.